

The established meteor showers as observed by CAMS



P. Jenniskens^{a,b,*}, Q. Nénon^a, J. Albers^a, P.S. Gural^c, B. Haberman^a, D. Holman^a, R. Morales^d, B.J. Grigsby^{a,e}, D. Samuels^d, C. Johannink^f

^aSETI Institute, 189 Bernardo Avenue, Mountain View, CA 94043, USA

^bNASA Ames Research Center, Mail Stop 241-11, Moffett Field, CA 94035, USA

^cLeidos, 14668 Lee Road, Chantilly, VA 20151, USA

^dFremont Peak Observatory Association, P.O. Box 1376, San Juan Bautista, CA 95045, USA

^eLick Observatory, U.C. Santa Cruz, 7281 Mount Hamilton Road, CA 95140, USA

^fDutch Meteor Society, Schiefstrasse 36, D 48599 Gronau, Germany

ARTICLE INFO

Article history:

Received 18 February 2014

Revised 23 August 2015

Accepted 2 September 2015

Available online 15 September 2015

Keywords:

Meteors

Comets, dust

Interplanetary dust

Near-Earth Objects

Asteroids

ABSTRACT

Orbital elements are presented for 70 of the 95 meteor showers considered “established” by the International Astronomical Union. From 2010 October 21 until 2013 March 31, the low-light-video based *Cameras for Allsky Meteor Surveillance* project (CAMS) measured a total of 110,367 meteoroid trajectories and pre-atmospheric orbits from mostly -2 to $+4$ magnitude meteors with a precision of $<2^\circ$ (median 0.4°) in apparent radiant direction and $<10\%$ (median 0.9%) in speed. This paper discusses how the already established showers manifest in this data. Newly resolved components in the radiant distribution shed light on the dynamics and physical lifetime of parent bodies and their meteoroids. Many multi-component showers have associated parent bodies with nodal lines not much rotated from that of their meteoroids (Encke Complex, Machholz Complex, Phaethon Complex, and now also the 169P/NEAT Complex). These may result from a parent body disruption cascade, with the disruption-generated meteoroids fading on the short timescale of a few hundred to a few thousand years. In particular, the Northern and Southern Taurids of the Encke Complex are decomposed here into 19 individual streams. Seven of these streams can be paired with mostly sub-km sized potential parent body asteroids that move in 2P/Encke-like orbits that span the narrow semi-major axis range of 2.20–2.35 AU. The meteoroids in these Taurid streams do not survive long enough for the nodal line to fully rotate relative to that of their parent body.

© 2015 Elsevier Inc. All rights reserved.

1. Introduction

The International Astronomical Union's Working List of Meteor Showers¹ included 495 meteor showers at the end of March 2013, but only 95 “established” showers were certain to exist (Jenniskens et al., 2009; Williams, 2011; Jopek and Kanuchová, 2014). Each established shower is evidence of past activity of a parent comet or asteroid, tracing its mass loss and dynamics. Many parent bodies are only now being discovered by the ongoing Near-Earth Object surveys (Jenniskens, 2006). A good understanding of the meteoroid streams at Earth fuels planetary science and planetary defense studies and is essential for satellite impact hazard mitigation.

The *Cameras for Allsky Meteor Surveillance* (CAMS) project was conceived to validate as many as possible of the 400 unconfirmed showers (Jenniskens et al., 2011a). To achieve that goal, CAMS scaled up existing techniques for measuring meteoroid trajectories from multi-station video imaging of meteors (Clifton, 1973; Hawkes and Jones, 1975; Jobse and de Lignie, 1987; Molau, 1993; Gural, 1995; Kotten et al., 2003; Koschny et al., 2004). The velocity vector and time of arrival are measured using 60 video cameras spread over three stations in California ($+37^\circ\text{N}$, 122°W). The resulting catalogue of meteoroid orbits is then used to search for groups of meteoroids arriving on orbits similar enough to originate from a common parent body (Southworth and Hawkins, 1963; Galligan, 2003; Jenniskens, 2006; Jopek et al., 2008; Veres and Tóth, 2010; Rozek et al., 2011).

CAMS does so very efficiently, in part because an operator evaluates the quality of each triangulation. In the period from October 2010 to March 2013, during the first 2.5 years of operation, CAMS measured over 100,000 meteoroid orbits in a uniform manner,

* Corresponding author at: SETI Institute, 189 Bernardo Avenue, Mountain View, CA 94043, USA. Fax: +1 650 962 9419.

E-mail address: Petrus.M.Jenniskens@nasa.gov (P. Jenniskens).

¹ <http://www.astro.amu.edu.pl/~jopek/MDC2007/>.

with a median precision slightly better than that of other ongoing video-based multi-station meteoroid orbit surveys (Jenniskens et al., 2011a).

In this paper, we focus on how CAMS detected showers that are already in the IAU List of Established Showers based on other techniques such as photography and radar. CAMS is a significant improvement on the photographic surveys of the past. Many showers established based on photographic data are still in need of accurately determined orbital elements (Jenniskens, 2006, Table 7). Video-based surveillance techniques capture much larger numbers of meteoroid trajectories per hour of observing time, so that streams stand out better from the sporadic background and stream dispersion and components are better defined.

Compared to radar-based surveys such as CMOR (Brown et al., 2008a,b, 2010) that detect fainter meteors (smaller meteoroids) of which there are more, CAMS often detects different showers and is sometimes more sensitive to younger stages of meteoroid stream evolution. Meteor outbursts from crossing cometary dust trails and resonant filaments are frequently detected. CAMS is also comparatively more sensitive to fast (>50 km/s apparent speed) and very slow (<20 km/s) meteors than the radar-based surveys.

CAMS is also well suited to validate results from other ongoing video-based meteoroid orbit survey. The SonotaCo network in Japan has measured meteoroid orbits at a yield of about 25,000 per year since 2007 (Kanamori, 2009). In Europe, the single-station IMO Video Meteor Network is collecting 350,000 (and rising) apparent meteoroid paths in the sky annually (Molau and Barentsen, 2014). As of 2013, 83,369 of these were triangulated and included in the European Video Meteor Network Database EDMOND (Kornos et al., 2012, 2014; Hajduková et al., 2014). Several smaller efforts are ongoing such as, for example, the Croatian Video Network (Vida et al., 2012; Gural et al., 2014). Unlike many of these surveys, CAMS is well documented and has been very uniform both in its data collection and reduction process.

In an earlier paper, we presented the first two months of CAMS observations and the techniques and methods used (Jenniskens et al., 2011a). In this paper, we discuss how the network has evolved since, and present the first 2.5 years of data. Results include median orbital elements for 70 already established nighttime northern hemisphere showers, newly detected shower components, and the detection of meteor outbursts, which provide insight into the dynamical evolution of parent bodies and their meteoroid streams.

2. Methods

Hardware, software, and operational procedures were described in detail in Jenniskens et al. (2011a). The hardware consists of three stations, each containing 20 narrow field-of-view low-light-level *Watec Wat 902H2 Ultimate* video cameras in a weatherproof box. Each station is equipped with a roll-off shutter and contains 19 cameras affixed with a 12-mm *f*/1.2 *Pentax* lens, each with a $30^\circ \times 22^\circ$ field of view, plus one zenith camera with a wider 8-mm *f*/1.4 lens ($45^\circ \times 33^\circ$ field of view), together covering the sky above $\sim 30^\circ$ elevation. Since Nov 27, 2011, these stations are located at Fremont Peak Observatory in Fremont Peak State Park ($+36.8^\circ\text{N}$, 121.5°W), Lick Observatory on Mount Hamilton ($+37.3^\circ\text{N}$, 121.6°W), and at a private residence in Sunnyvale (37.3°N , 122.0°W). The sites are 54–64 km apart. The cameras that contribute to a meteor trajectory are recorded, and the effective survey area is known at all times.

In addition to the three main stations, the CAMS software tools have now been adapted for use on PC, so that amateur astronomers can contribute their own single-CAMS cameras. As of March 2013, three amateur-run single-CAMS stations had come online as part of

the California network, each contributing 1–2 cameras, as did a small but growing network of single-CAMS cameras operated in the Netherlands and Belgium (the CAMS@BeNeLux network). They use the same camera and lens configuration to maintain consistent angular resolution. These additional cameras made only a small contribution to the data presented here, but are expected to generate significant yield in the future.

The new single-CAMS software tools include online image processing. Since October 2012, the main stations now also perform image processing on-site, but off-line after each night of observations. The detection algorithms and modules from the MeteorScan software package (Gural, 1995, 1997) are used to detect the meteors and retrieve the astrometric data. The software works on video sequences of 256 frames (NTSC, 29.97 frame-per-second) that are written in a compressed “Four-Frame” format, consisting of 4 video frames that report for each pixel the value for the peak intensity, the frame number in which this occurred, the average temporal intensity, and the associated standard deviation. This saves the temporal propagation history of the meteor and preserves the astrometric accuracy for equatorial coordinate calibration. The 8-s averaged frames typically contain 70–200 stars of +8.1 and brighter, with sub-pixel (~ 1 arcmin) fitting residuals when employing a cubic polynomial warp in the gnomonic coordinate frame, and ± 0.3 magnitude photometric accuracy against the star background. The photometry is corrected for saturation above +1 magnitude, reliable down to about magnitude -5 , in a +5.4 stellar limiting magnitude single frame (Jenniskens et al., 2011a).

After reprocessing of the video frames to extract the astrometric position of the meteor, all tracks were gathered in the analysis facility at the SETI Institute, where software for calibration and multi-station coincidence processing combine the data and produce atmospheric trajectories and orbital elements (Jenniskens et al., 2011a). The internet-connected single-CAMS cameras provided the absolute time to about ± 1 s, while relative time offsets were calibrated from coincident meteor detections. The Coincidence software is interactive, adding an element of quality control. Each trajectory and light curve solution is projected on-screen, with different colors showing the contribution of each contributing camera. The result is accepted or rejected by an operator based on the lightcurve (brightness versus altitude), a side view of the trajectory (altitude versus downrange), and a top view of the trajectory (latitude versus longitude). Each operator-accepted meteor was only accepted if two selection criteria were met: an apparent radiant better than 2° and apparent speed better than 10%. This removed unacceptably poor tracks and most incorrect solutions that slipped by the operator.

In a modification to earlier reported methods, the data presented here (including previously reported results) were re-calculated with Coincidence version 1.3, in which the trajectory is calculated first by using the intersecting planes method of Cepelcha (1987) and refined using the individual lines of sight to the meteor in sequential video frames. We use the constant frame rate and relative time difference to other cameras in a new approach to combine the data from multiple stations (Gural, 2012).

As a model for the changing observed velocity $V_o(t)$ of the meteoroid moving along the fitted line, we use the empirical equation proposed by Whipple and Jacchia (1957) and Jacchia et al. (1961), which consists of an initial deceleration $a_1 a_2^2$ at $t = 0$, which then exponentially increases as defined by the constant a_2 . Resulting initial velocities are in good agreement with those expected for meteoroids moving close to the parabolic limit (Jenniskens et al., 2011a). As a correction to Eq. (5a) in Jenniskens et al. (2011a), please note that the term “ $+a_1 a_2$ ” in Eq. (5a) is included in the definition of the apparent entry speed V_∞ as tabulated in the meteoroid trajectory and orbit data provided to the Meteor Data Center. The correct equations are (Jacchia et al., 1961):

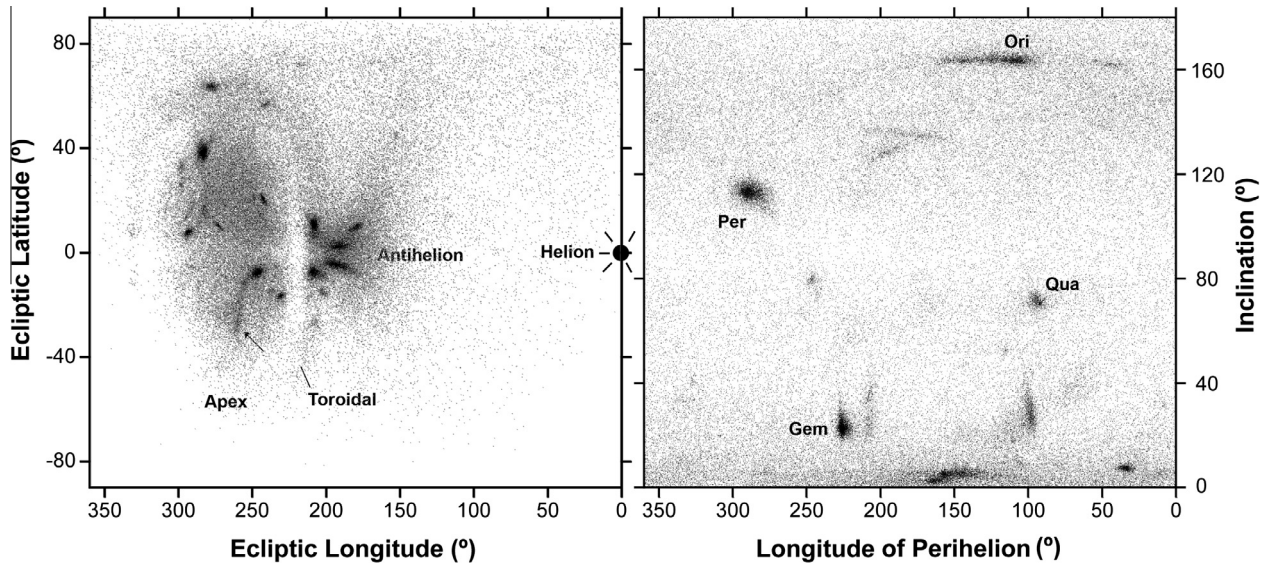


Fig. 1. Left: Approach direction of CAMS-detected meteoroids in sun-centered ecliptic coordinates. Source regions are identified. The small arrow points to the “Orionid tail”, a newly recognized shower complex. Right: Distribution of orbital elements II and i . The Perseid (Per), Orionid (Ori), Geminid (Gem) and Quadrantid (QUA) showers are identified.

$$d_o(t) = d(t = 0) + V_\infty t - |a_1| \exp(a_2 t) \quad (1)$$

$$V_o(t) = V_\infty - |a_1 a_2| \exp(a_2 t) \quad (2)$$

$$A_o(t) = -|a_1 a_2^2| \exp(a_2 t) \quad (3)$$

where $d(t)$ is the distance along the meteor trajectory as a function of time, starting from the beginning point of the first recorded trail at time $t = 0$, and $A_o(t)$ the observed instantaneous acceleration. Here, we force the solution to converge on positive values of a_1 (unit: km) and a_2 (unit: s^{-1}). A Monte-Carlo approach is taken to understand how the uncertainties in measurement errors propagate in the trajectory solution, speed and deceleration.

Once the trajectories and pre-atmospheric orbits have been calculated, each measured orbit is compared to that of the listed orbital elements in the IAU Working List of Meteor Showers. The similarity of each orbit to the reference orbit is calculated using the D_h discriminant criterion (Jopek, 1993), implemented in a new interactive data analysis application called *CAMS StreamFinder*. This tool makes it possible to adjust the threshold parameter that separates stream meteoroids from sporadics, or the reference orbit, to select only the stream excess phase space density in diagrams such as shown in Fig. 1. The left diagram plots the sun-centered ecliptic radiant coordinates, while the right diagram shows the orbital element space of inclination (i) versus longitude of perihelion (II). The sun-centered coordinates are derived from the ecliptic radiant coordinates (λ, β) by removing the drift from Earth’s motion around the Sun: $\Delta\lambda = -1^\circ$ and $\Delta\beta = 0^\circ$ per degree solar longitude (λ_o). By also considering the distribution of orbital elements i and II , we limit the accepted range of entry speed, thus isolating groups of radiant position, entry speed, and time.

This approach ignores tails in the population distribution of streams that fall below the sporadic background, and excludes shower orbits with erroneously high or low entry speed measurements, but avoids ambiguity about the threshold parameter and does not extract random sets of similar orbits in an otherwise homogeneous sporadic background.

A number of showers were found to have multiple components. Each component was given a separate name and IAU number, following established practices in which, for example, the various Taurid showers carry individual names. These may well originate from different parent bodies. Separate components may also arise

if a group of meteoroids has a distinctly different dynamical history from the main component due to the action of mean motion resonances, for example, or because of distinctly different physical properties. If proven so, the proposed new name may be unnecessary.

3. Results

The extracted stream members are identified by their IAU Working List stream number in the CAMS Meteoroid Orbit Database 2.0, which contains all measured orbits up to March 31, 2013. The database can be accessed at the IAU Meteor Data Center. This identification makes it possible to reproduce what meteor orbits were selected for an individual meteor shower or shower component and to clarify the meteor shower nomenclature used here, if needed.

3.1. Level of survey completeness

Fig. 1 provides an overview of all measured data. Meteoroids from the apex and the antihelion sources are detected in about equal numbers. Because the survey is conducted at $37^\circ N$ latitude and in nighttime, the helion source (daytime showers) and southern toroidal source (southern hemisphere showers) remain mostly undetected.

The California CAMS stations measured a total of 109,548 trajectories and orbits. The CAMS@BeNeLux network added another 973. Most meteors had an apparent brightness between -2 and $+4$ magnitude (median $+1.2$ magnitude). Of these, 154 were found to be duplicates (leaving a combined 110,367 unique trajectories). Duplicates are combinations of the same meteor observed by different pairs of cameras. Because of the manner in which the velocity profile is determined, this data cannot be simply averaged to get a more accurate orbit. Instead of removing the duplicates, those with the larger error are flagged in the data file. Duplicates are not counted in the number of meteors reported for each extracted stream.

On average, the effective surface area covered by the CAMS cameras in California is $35,949 \text{ km}^2$. The effective nightly sky coverage, expressed in terms of area covered by each camera times the hours of operation, summed over all active cameras, has been fairly

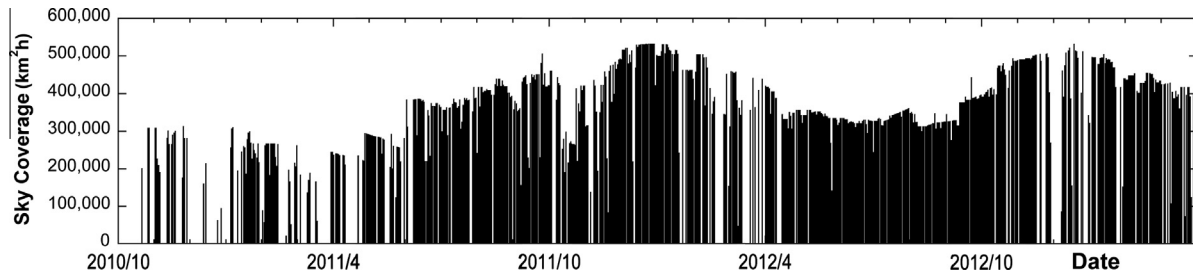


Fig. 2. The effective nightly sky coverage, defined as the combined number of clear sky camera hours and effective surface area covered by each camera.

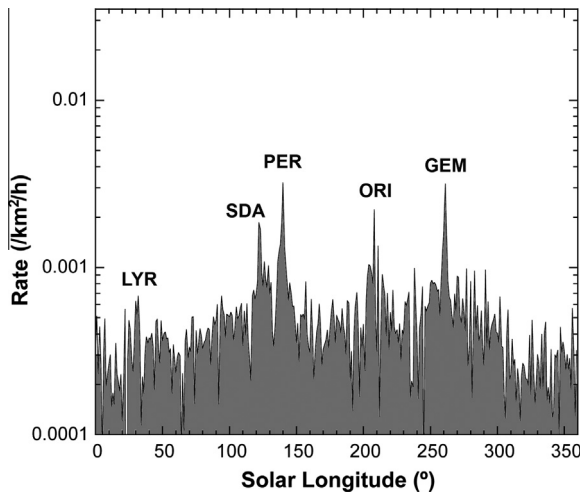


Fig. 3. The mean clear-sky hourly meteor rate throughout the year.

constant since the third (Lick Observatory) station came online on April 28, 2011 (Fig. 2). Longer nights in winter months permit more hours of observation. There were 664 (partially) clear nights in the period from October 21st, 2010 until March 30th, 2013.

Solar longitude (λ_o) measures the position of Earth in its orbit. The accumulated solar longitude coverage is shown in Fig. 3. The anticipated yield was about 300 meteors per solar longitude interval of 1° in a 3-year survey (Jenniskens et al., 2011a). At the end of March, 2013, the yield has reached 302 meteors per interval on average, but higher rates are detected in autumn than in springtime. Thanks to generally good weather conditions, 300 or more meteors were detected for 155 out of the 360 intervals. Only 44 one-degree λ_o intervals have less than 100 meteors and 13 have less than 30 meteors, namely $\lambda_o = 7, 21\text{--}24, 34, 56, 64, 66, 330, 331, 334, \text{ and } 359$. Clouds are mainly a problem in the months of November through April.

3.2. Accuracy

The distribution of measurement uncertainties is wide. The uncertainty in the radiant angle is on average $\pm 0.40^\circ$ (median value), with a standard deviation of 0.42° . As much as 85% of trajectories have an uncertainty in the radiant position less than 1° , the target precision of CAMS. The median value of uncertainty for entry speed (V_{inf}) was 0.89%, respectively, or ± 0.37 km/s, errors being distributed with a standard deviation of $\sigma = 0.76$ km/s. 82% of trajectories have an error less than 1 km/s, the target precision of CAMS.

The geocentric parameters for radiant and speed reported in this paper are derived after removal of the effects from Earth's rotation and the acceleration due to Earth's gravity (Jenniskens et al., 2011a). The error in the geocentric speed (V_g) is not much

changed by this, amounting to about ± 0.26 km/s for $V_g = 10$ km/s meteors, rising to about ± 0.63 km/s for fast 70 km/s meteors. However, errors in entry speed add uncertainty to the correction for zenith attraction, resulting in a median uncertainty of $\pm 0.77^\circ$ ($\sigma = 1.54^\circ$) in the geocentric radiant position, rising to as large as $\pm 30^\circ$ when $V_g \ll 10$ km/s. 61% of the geocentric trajectories have an uncertainty less than $\pm 1^\circ$ in radiant position.

Meteoroid orbits with large errors tend not to be assigned to streams. For those meteors that are assigned to the established meteoroid streams, the geocentric radiant has a median uncertainty of $\pm 0.39^\circ$ in R.A. ($\sigma = 0.74^\circ$) and $\pm 0.56^\circ$ in Decl. ($\sigma = 0.64^\circ$), while the speed is uncertain by ± 0.37 km/s ($\sigma = 0.72$ km/s). 68% of trajectories have an uncertainty less than $\pm 1^\circ$.

3.3. Median orbital elements

Meteor showers stand out as clusters in the diagram of Fig. 1. Because we focus our attention here on the established showers, the task at hand is to extract the relevant cluster at the expected radiant and velocity coordinates and measure the median orbital elements of the extracted meteoroids, the precision of their measurement and the dispersion in their values (Jopek et al., 2006).

The median orbital elements of 70 established showers are presented in Tables 1–12 and the individual detections are discussed in Section 4. The measured precision of the median radiant position and speed, as well as the dispersion of these parameters, is given in Table 13. The semi-major axis (a) represents the inverse of the median of $1/a$. When that median is less or equal to zero, the value is given as “Inf.”

The radiant is drift-corrected to an integer solar longitude value, chosen nearest to the median solar longitude of the observed stream or based on a previously reported shower peak. The radiant drift rate in Table 13 can be used to calculate the radiant at a different solar longitude.

Also given in Table 13 is the stream-to-background (S/B) surface density ratio, which is the number of assigned stream members inside the 2σ contour of the distribution over that in the nearby background (both unassigned and previously assigned meteors), averaged over a four times bigger area. $S/B = 1$ means that the shower raises the local surface density a factor of two above the sporadic background. Typically, $S/B \leq 2$ would constitute tentative detections, while values larger than 3 are strong detections.

4. The established showers

4.1. The α -Capricornids

This ecliptic low-inclination shower was discovered based on only 12 photographic orbits from the Harvard Meteor Orbit Survey (Wright et al., 1956). The shower was recently associated with weakly active Comet 169P/NEAT (Jenniskens, 2006; Jenniskens and Vaubaillon, 2010), which has a $D = 1.4$ -km diameter based on the comet's absolute nuclear magnitude H_N

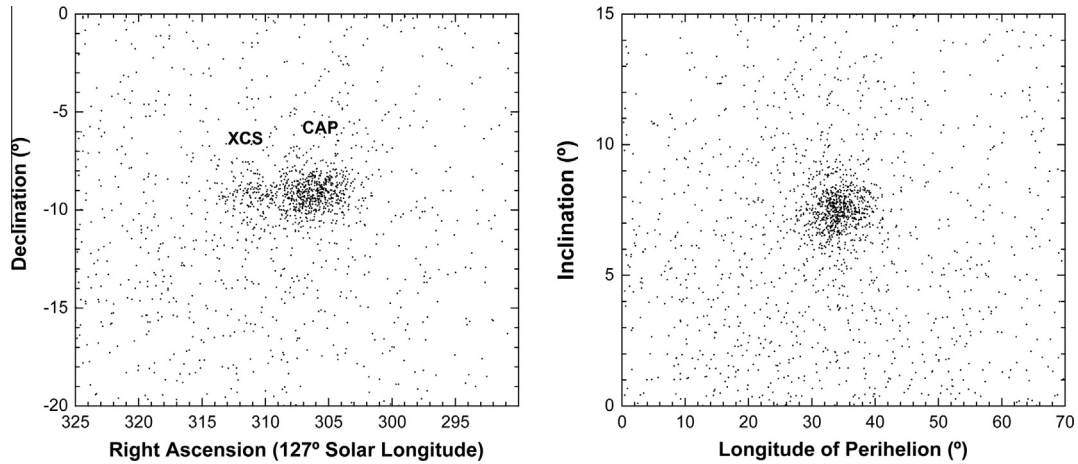


Fig. 4. Alpha Capricornids – radiant positions in equatorial coordinates toward the antihelion source direction during $\lambda_o = 104\text{--}134^\circ$, drift-corrected to solar $\lambda_o = 127^\circ$. The newly identified ξ^2 -Capricornid (XCS) are not distinguished in the II - i diagram (right).

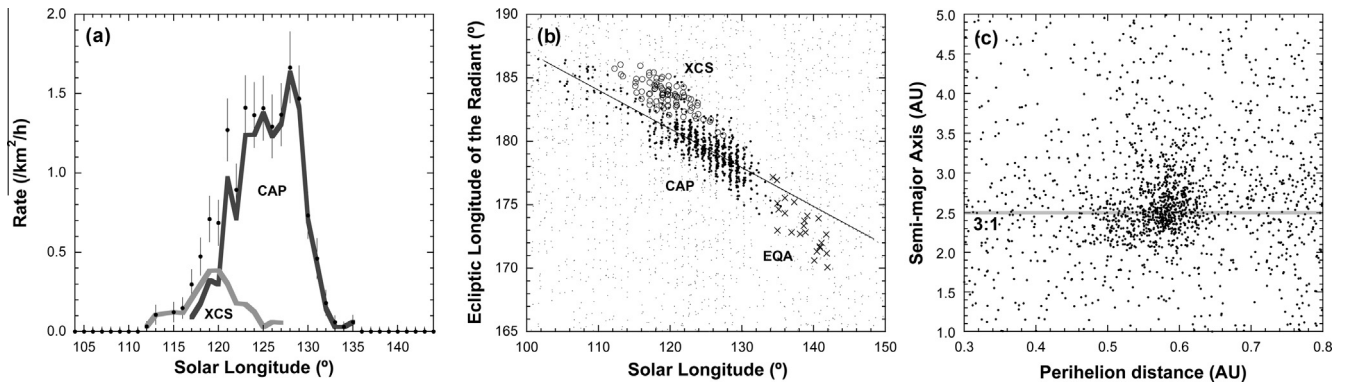


Fig. 5. Alpha Capricornids – (a) rate profile of the α -Capricornids (CAP) and ξ^2 -Capricornids (XCS), with solid dots showing the combined activity. (b) Radiant drift with least squares fit through the α -Capricornids. The ε -Aquiriids (EQA) are shown as crosses. (c) Semi-major axis versus perihelion distance for all meteors during $\lambda_o = 113\text{--}134^\circ$. The 3:1 mean-motion resonance with Jupiter is marked.

and assuming a geometric albedo $\alpha = 0.04$, using $\log D$ (km) = $3.12 - 0.200H_N - 0.05 \log(\alpha)$ (Plavec and Harris, 2007).

CAMS measured 646 video orbits for the main component of the α -Capricornids (IAU#1, CAP). The stream number 1 indicates the order in which this shower is listed in the IAU Working List of Meteor Showers, while “CAP” is the assigned three-letter code.

The distribution of meteors in the two CAMS *StreamFinder* graphs are plotted in Fig. 4. The shower stands out well from the sporadic background and the dispersion is resolved. The drift-corrected radiant distribution of the CAP is compact at its core $\lambda_o = 123\text{--}125^\circ$, and more diffuse at other times. The shower activity

curve, the number of shower members detected per hour of observation as a function of solar longitude, has a centroid at $\lambda_o = 125.6^\circ$ (Fig. 5a). There is a residual radiant drift toward shorter ecliptic longitudes with increasing solar longitude (Fig. 5b).

CAMS data also detected a second component in the drift-corrected radiant (Fig. 4a), which we will refer to as the ξ^2 -Capricornids (#623, XCS). The radiant positions form a narrow arc at an angle to the ecliptic plane (Fig. 4a). The new component has 86 members with threshold $D_h \leq 0.065$ and is active from $\lambda_o = 113^\circ$ to 124° (Fig. 5a). This is a strong detection, with a radiant number density inside the 2σ contour that is 28 times that over the

Table 1
The α -Capricornids – median orbital elements of meteor shower components.

IAU ^a	Object	<i>N</i>	λ_o	R.A.	Dec.	V_g	<i>a</i>	<i>q</i>	<i>e</i>	<i>i</i>	ω	Node	<i>II</i>	T_J
1	CAP	646	127	306.5	−9.2	23.0	2.54	0.578	0.774	7.5	268.9	125.4	33.7	2.92
	*169P	A	127.9	305.7	−9.5	22.1	2.60	0.607	0.767	6.9	265.8	127.9	33.7	2.89
623	XCS	86	120	303.9	−10.8	24.5	2.40	0.509	0.786	7.6	277.4	119.7	37.3	3.00
	*2003 T12	A	124.0	303.9	−10.5	23.0	2.57	0.575	0.776	7.0	269.6	124.0	33.6	2.89
692	EQA	23	138	310.5	−5.8	19.9	2.50	0.685	0.729	7.4	256.9	138.7	35.5	3.02

^a In this and following tables, the header symbols have the following meaning: IAU number; object = IAU meteor shower code or parent body designation (with parent bodies labeled “*” = probable or “?” = possible); *N* = number of observed meteors; λ_o = median solar longitude of the distribution; position of the radiant: R.A. = Right Ascension and Dec. = Declination (°, J2000); V_g = geocentric entry speed in km/s (without Earth’s gravitational acceleration); orbital elements in equinox J2000: *a* = semi-major axis (AU), *q* = perihelion distance (AU), *i* = inclination (°), ω = argument of perihelion (°), node = ascending node (°), *II* = longitude of perihelion (°); T_J = Tisserand parameter with respect to Jupiter. The parent body orbit is adjusted to intersect Earth’s orbit by rotating around the line of apsides, using method “A” of Neslusan et al. (1998) as indicated in column 3. Other methods used here: H = Adjustment by variation of the argument of perihelion and inclination; P = Adjustment from a parallel shift of the velocity vector; Q = Adjustment by variation of the perihelion distance; W = Adjustment by variation of the argument of perihelion.

nearby sporadic background. The average speed of the XCS is slightly higher than that of the main component: $V_g = 24.5 \pm 0.1$ versus 23.0 ± 0.1 km/s.

There is also a third component. The α -Capricornid activity drops off rapidly at $\lambda_o = 133^\circ$ (Fig. 5a), but the shower is known to be active even during the peak of the Perseids around $\lambda_o = 140^\circ$ (Jenniskens, 1994). Indeed, CAMS detects a tail of activity in the period $\lambda_o = 134\text{--}142^\circ$ with a drift-corrected radiant displaced from that of the α -Capricornid shower (Fig. 5b). For that reason, they were given a separate name, the ε -Aquiriids (#692, EQA). 23 members were isolated and the median orbital elements are given in Table 1.

4.2. The Encke Complex

Even based on the sparse photographic orbits, the Southern Taurids (#2, STA) and the Northern Taurids (#17, NTA) are thought to be composed of several components (Porubcan et al., 2006; Babadzhanov et al., 2008; Bucek and Porubcan, 2014). Our sun-centered ecliptic Taurid shower radiants move from high to low ecliptic longitude with increasing solar longitude (Fig. 6). This drift is not continuous, with early Taurids drifting more gradually with solar longitude (Fig. 6). Just after $\lambda_o = 235^\circ$, the Southern Taurid component continues to drift to lower ecliptic longitude and a separate component emerges at a higher ecliptic longitude (Fig. 7). The newly emerging stream is established and known as the Southern χ -Orionids (#257, ORS).

Overall, Southern and Northern Taurid activity is not symmetric in solar longitude (Fig. 6). That means that the Northern and Southern Taurids are not strict twin showers, in the sense that they have activity at the corresponding twin node because precession will rotate the nodal line. It was known from photographic observations that the Southern Taurids are more pronounced in October and early November, while the Northern Taurids are more active in the middle and later part of November (Porubcan et al.,

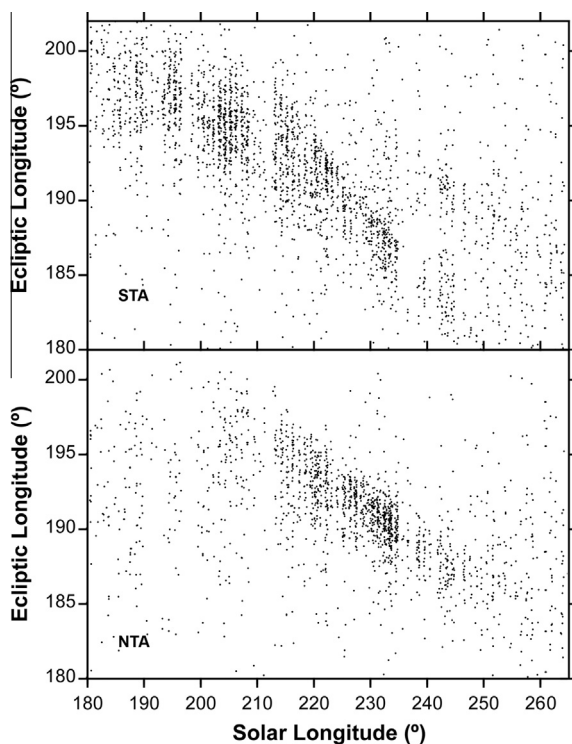


Fig. 6. Taurids – radiant drift of Southern Taurids (STA, top) and Northern Taurids (NTA, bottom) during $\lambda_o = 180\text{--}265^\circ$. Gaps are due to adverse weather.

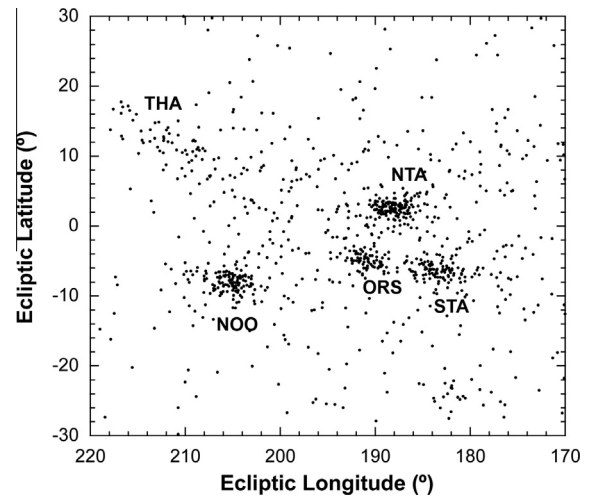


Fig. 7. Southern χ -Orionids – radiants during $\lambda_o = 235\text{--}245^\circ$, when the Southern χ -Orionids (ORS) emerge at a distinct position from the Southern Taurids (STA). Other showers shown in this diagram are the Northern Taurids (NTA), the November Orionids (NOO) and the θ -Aurigids (THA).

2006; Jenniskens, 2006). This is evident also in the CAMS observations (Fig. 6).

The Northern and Southern Taurid radiant show differences in relative activity and compactness of the radiant from day to day (Fig. 8). On some days the Northern Taurids are more active, while on other days the Southern Taurids dominate. It is not clear at present whether these patterns repeat from year to year.

It appears that the drift-corrected radiant position is unchanged for a few days, then jumps to a next position. In Fig. 8, for example, the Northern Taurid radiant appears to jump at $\lambda_o = 224^\circ$, while the Southern Taurid radiant appears to jump at $\lambda_o = 225^\circ$, then again at $\lambda_o = 229^\circ$. Jumps look like the result of chance changes in the scatter of Taurid meteors from day to day, but between jumps the radiant becomes more compact and then more diffuse again, while overall rates appear to climb and fall even after correcting for the effective observing time (Fig. 9).

Assuming that these apparent jumps are not due to observational effects such as low-number statistics combined with adverse weather conditions on some days, the individual components were extracted by placing a small circle of 1° diameter on the visually identified cluster of drift-corrected radiants. The mean orbit for this sample was then used to extract the component using the D_{sh} criterion (Southworth and Hawkins, 1963) with threshold values of 0.06–0.09. In this case, D_{sh} and D_h (Jopek, 1993) gave similar results, while other criteria (e.g., D_n of Valsecchi et al., 1999) did not improve the extraction of the cluster.

Table 2 lists the average orbital elements of a total of 19 Taurid components. The typical duration of each component is 3–10 days, much like the activity profile of the α -Capricornids, for example (Fig. 5a). Gray and dark lines in Fig. 9 trace the activity of individual components. Dots show the total Taurid activity in the September to December period ($\lambda_o = 160\text{--}280^\circ$). Visual observers recognize activity in the range $\lambda_o = 190\text{--}260^\circ$, in good agreement (Jenniskens, 1994; Dubietis and Arlt, 2007).

Toward lower and higher longitudes, the Southern Taurids appear to be still active at a weak level, but not enough meteors were observed to recognize individual components. Taurids that were not assigned to the subcomponents listed in Table 2, were assigned to shower #2 (Southern Taurids) or #17 (Northern Taurids), instead.

The name Southern October δ -Arietids (#28, SOA) was assigned to one of the Southern Taurid shower components, most similar to

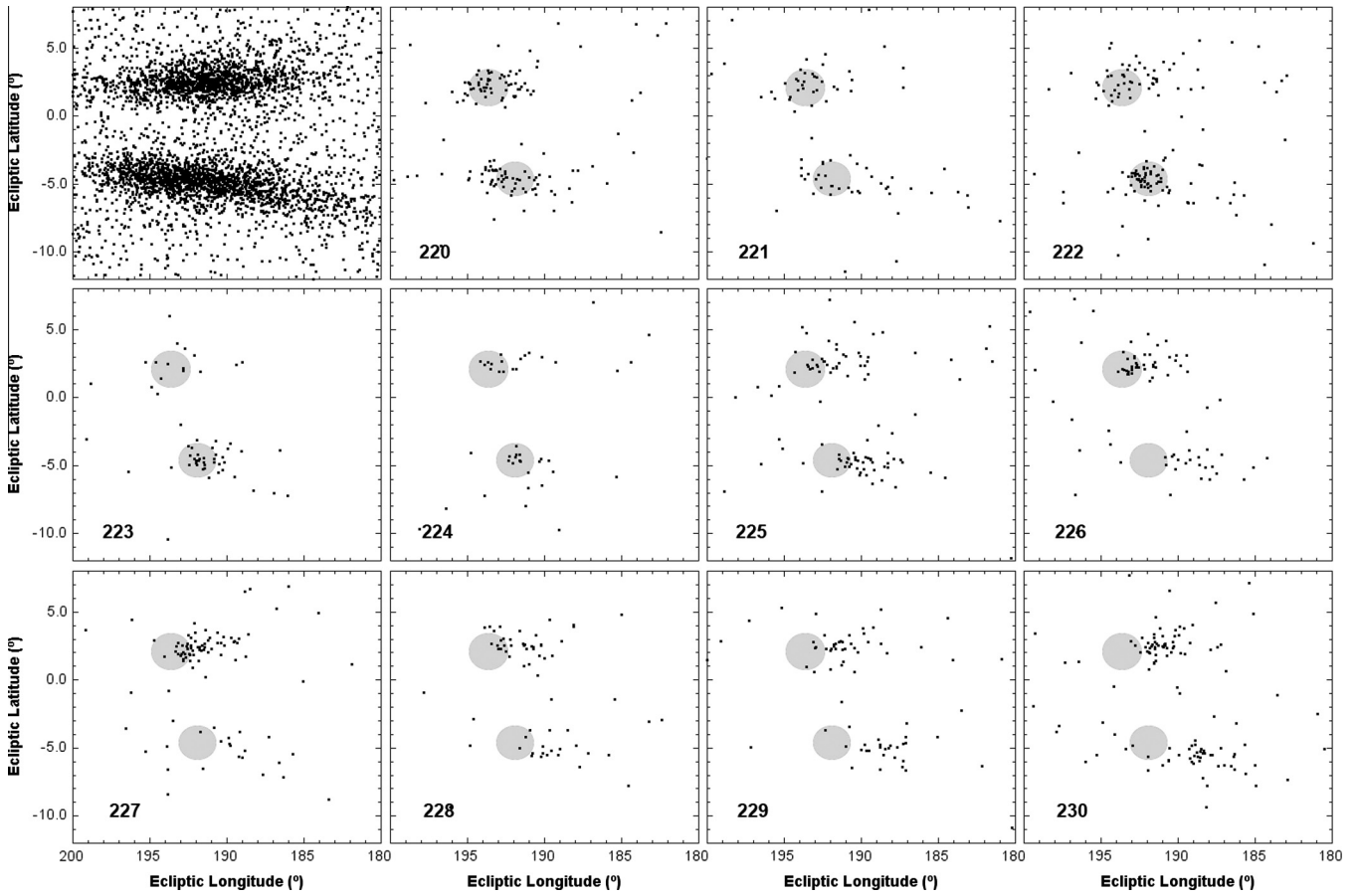


Fig. 8. Taurids – radiant position in sun-centered ecliptic coordinates, showing all meteors in the period $\lambda_0 = 190\text{--}260^\circ$ (top, left), as well as the daily radiant maps for $\lambda_0 = 220\text{--}230^\circ$. The two gray areas are plotted at a constant position in the diagram to show the intrinsic radiant drift.

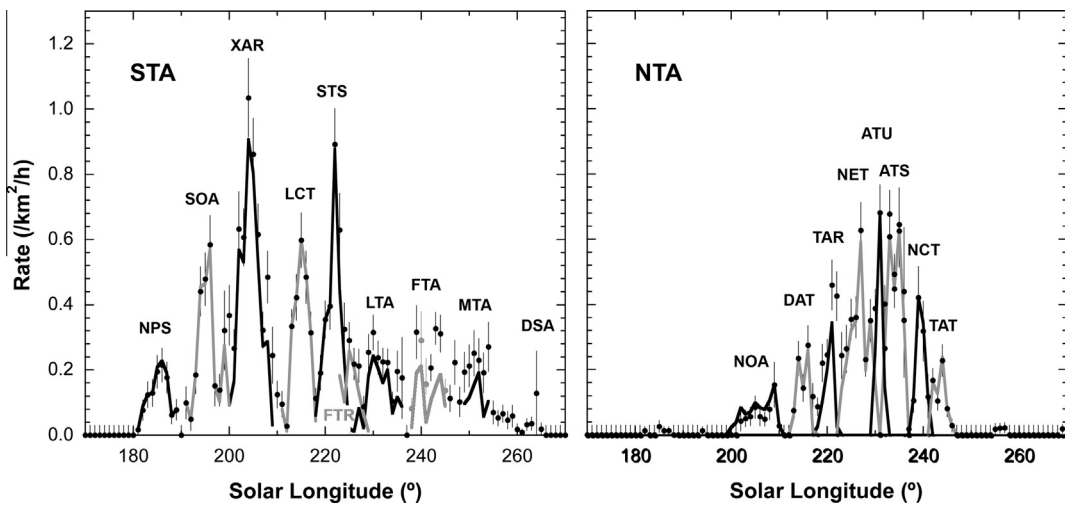


Fig. 9. Taurids – shower activity for all Taurids (•) and for individual shower components defined in the text (gray and dark lines).

orbital elements claimed for this stream in the past (Sekanina, 1976; Jenniskens, 2006). Note that this shower name originally was intended to encompass most Encke Complex meteor activity in October (Jenniskens, 2006). In the same way, the name Northern October δ -Arietids (#25, NOA) was assigned to one of the Northern Taurid shower components.

4.3. Possible late and early Encke Complex showers

It is not clear how the Southern χ -Orionids relate to the Southern Taurids. They do have the same semi-major axis $a = 2.22$ AU and longitude of perihelion ($\Pi \sim 158^\circ$) typical of other Taurid shower components, but they deviate from the general trend of

Table 2
The Encke Complex – Northern and Southern Taurid shower components.

IAU	Object ^a	<i>N</i>	λ_o	R.A.	Dec.	V_g	<i>a</i>	<i>q</i>	<i>e</i>	<i>i</i>	ω	Node	Π	T_j
\pm	Uncertainty	–	0.2	0.2	0.1	0.1	0.03	0.003	0.002	0.1	0.3	0.2	0.4	0.10
σ	Dispersion	–	3.8	2.6	2.5	1.1	0.06	0.029	0.022	1.3	3.1	1.9	3.8	0.32
<i>Southern</i>														
627	NPS	87	189	25.5	+6.8	29.4	1.73	0.276	0.842	5.0	125.8	5.6	130.9	3.63
28	SOA	149	196	32.0	+8.5	29.0	1.75	0.286	0.834	5.7	124.6	15.4	139.8	3.61
624	XAR	290	205	39.1	+10.5	28.5	1.86	0.312	0.830	5.7	120.9	24.4	145.7	3.47
626	LCT	194	216	48.1	+13.1	27.9	1.94	0.345	0.821	5.5	116.5	35.1	151.7	3.38
	*2010 TU149 ^r	<i>H</i>	220.1	48.7	+16.3	27.7	2.20	0.378	0.828	1.9	111.5	40.1	151.6	3.09
628	STS	199	223	53.8	+14.4	28.2	2.13	0.358	0.831	5.5	114.1	42.1	155.9	3.15
	Outburst 7:2 ^b	139	222	53.0	+14.1	28.0	2.26	0.358	0.828	5.5	114.4	42.5	156.9	3.04
	*2P/Encke	<i>H</i>	224.6	55.9	+16.4	29.1	2.22	0.336	0.848	4.0	116.1	44.6	160.5	3.03
637	FTR	61	225	54.1	+14.6	27.4	2.14	0.390	0.820	5.0	110.3	45.9	156.5	3.16
625	LTA	131	231	57.8	+14.8	25.7	2.13	0.439	0.793	5.1	104.8	51.3	156.5	3.22
286	FTA	81	242	65.2	+15.1	23.3	2.10	0.517	0.751	5.1	96.2	62.7	158.2	3.31
	*2003 WP21 ^j	<i>H</i>	243.4	67.0	+17.2	24.5	2.26	0.492	0.783	3.9	98.2	63.3	161.5	3.13
636	MTA	36	252	80.3	+17.8	27.4	2.21	0.411	0.816	5.5	106.9	71.5	178.8	3.11
288	DSA	13	265	74.4	+12.5	17.5	2.25	0.726	0.684	5.2	68.6	84.6	153.8	3.27
2	STA	916	216	47.9	+12.8	26.6	1.95	0.353	0.798	5.3	116.6	34.4	149.6	3.40
<i>Northern</i>														
25	NOA	53	205	38.6	+17.8	30.1	1.89	0.274	0.857	3.6	305.4	206.1	151.0	3.38
631	DAT	57	216	48.1	+20.4	29.3	1.94	0.300	0.846	3.2	301.8	215.2	156.4	3.33
630	TAR	59	220	50.0	+21.1	28.1	1.96	0.341	0.824	3.1	296.6	220.4	156.7	3.34
	*2005 TF50 ^o	<i>P</i>	219.5	51.5	+19.4	20.5	2.27	0.298	0.869	0.8	300.5	219.5	160.6	2.93
632	NET	194	227	56.1	+22.3	28.0	2.11	0.357	0.827	2.8	294.3	227.1	161.3	3.18
	*2004 TG10 ^j	<i>H</i>	223.2	54.3	+22.5	30.1	2.23	0.308	0.862	4.0	299.3	223.2	162.5	2.99
635	ATU	136	231	58.9	+22.8	27.4	2.16	0.381	0.819	2.6	291.2	231.2	162.3	3.15
629	ATS	206	233	60.7	+23.2	27.5	2.19	0.385	0.823	2.7	290.5	233.4	164.2	3.12
	*2012 UR158	<i>H</i>	228.5	59.3	+21.8	29.6	2.25	0.324	0.856	1.6	297.4	228.5	165.9	2.99
633	NCT	46	240	66.7	+24.1	26.7	2.21	0.413	0.812	2.5	287.2	238.6	166.5	3.12
634	TAT	70	244	69.7	+24.7	25.8	2.17	0.439	0.801	2.5	284.7	243.3	168.2	3.17
	*2003 UL3 ^p	<i>H</i>	243.4	68.5	+21.9	25.6	2.24	0.452	0.798	0.0	282.7	243.4	166.1	3.09
726	DEG	17	268	96.7	+25.6	26.8	2.26	0.420	0.816	2.3	285.6	268.0	194.2	3.07
17	NTA	509	220	48.9	+20.7	28.0	2.13	0.355	0.829	3.0	294.6	220.6	158.5	3.16

^a The header includes the typical uncertainty of determining the mean, as well as the dispersion of the orbital elements. Uncertainties are in terms of 1 standard deviation.

Notes: j = Jenniskens (2006); p = Porubcan et al. (2006); b = Babadzhanov et al. (2008); o = Ohtsuka (2006); and r = Rudawska et al. (2013).

^b Not observed by CAMS.

changing Π and q with solar longitude. The name Southern χ -Orionids (#257, ORS) was assigned here to the most prominent component of the branch known under that name (Fig. 7). Two later component of this branch were assigned the names m-Taurids (#636, MTA) and December ζ -Taurids (#638, DZT). Orbital elements are given in Table 3.

We assigned the name Northern χ -Orionids (#256, ORN) to one of the Northern Taurid shower components with orbital elements

similar to those derived from previously reported photographed ORN orbits (see Table 7 in Jenniskens, 2006).

Into January, there is still a concentration of radiants suggestive of Encke Complex showers in the antihelion source (Fig. 10). These now confirmed showers are known as the Northern δ -Cancriids (#96, NCC) and the Southern δ -Cancriids (#97, SCC). The diffuse northern branch is at a slightly lower inclination than the better-defined southern branch (Table 3). Again, the radiant travels to

Table 3
The Encke Complex – possibly related early and late showers.

IAU	Object	<i>N</i>	λ_o	R.A.	Dec.	V_g	<i>a</i>	<i>q</i>	<i>e</i>	<i>i</i>	ω	Node	Π	T_j
<i>Southern</i>														
642	PCE	23	161	8.2	−5.3	36.5	2.25	0.145	0.931	19.4	140.8	341.1	122.4	−
216	SPI	52	176	16.2	+2.8	28.6	1.45	0.251	0.826	5.6	132.8	353.9	127.9	4.19
257	ORS	97	243	73.0	+17.8	27.9	2.16	0.381	0.828	5.3	111.3	64.3	175.3	3.13
	*2010 LU108	<i>H</i>	248.7	76.7	+22.2	27.1	2.24	0.407	0.819	0.7	107.8	68.7	176.5	3.07
636	MTA	36	252	80.3	+17.8	27.4	2.21	0.411	0.816	5.5	106.9	71.5	178.8	3.11
638	DZT	51	260	86.4	+18.3	25.8	2.25	0.457	0.797	4.8	102.2	80.0	181.8	3.10
	?2008 ON13	<i>H</i>	263.0	92.2	+20.7	27.1	2.21	0.408	0.816	2.9	107.7	83.0	190.0	3.10
97	SCC	69	296	125.0	+14.4	27.0	2.26	0.430	0.811	4.7	105.0	109.3	215.4	3.07
<i>Northern</i>														
33	NIA	94	148	346.7	−1.2	31.3	1.76	0.234	0.874	5.9	310.5	147.8	97.9	3.51
	?2006 PF1	<i>H</i>	154.7	349.1	+4.1	31.5	2.19	0.267	0.878	12.3	305.0	154.7	99.7	2.98
215	NPI	77	176	10.2	+8.6	28.0	1.63	0.291	0.820	4.9	305.1	172.0	116.7	3.82
256	ORN	37	258	83.2	+25.7	24.7	2.09	0.473	0.778	2.2	280.8	255.9	177.6	3.27
	*2008 XM1	<i>H</i>	259.2	82.3	+29.0	24.6	2.36	0.500	0.788	5.0	276.7	259.2	175.9	3.03
96	NCC	74	296	127.6	+21.5	27.2	2.32	0.410	0.814	2.7	286.6	290.0	217.6	3.10

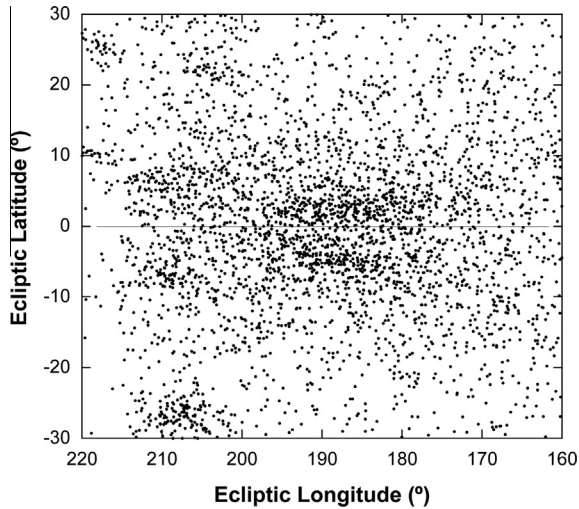


Fig. 10. Cancrids – the Northern and Southern Cancrids radiate from just above and below the ecliptic plane at the center of this diagram in late December and January ($\lambda_o = 268\text{--}306^\circ$).

lower ecliptic longitudes later in the month of January. Grouped in periods of five days, the distribution of meteor radiants varies significantly, suggesting that these streams, too, consist of more than one component.

Some Taurid-like activity extends also below $\lambda_o = 189^\circ$, into September and August. Early Southern Taurids are called the Southern Piscids (#216, SPI), but the shower does not separate well from STA activity. Table 3 lists orbital elements for 52 Southern Taurids assigned to this component. The Northern Taurids ramp up much later, so that the activity of the corresponding Northern Piscids (#215, NPI) is more clearly separated. This shower is recognized as a cluster centered on $\lambda_o = 174^\circ$, active over a period of about 11 days in September (Table 3). Even earlier than the Northern Piscids are the Northern ι -Aquiriids (#33, NIA). These are known to be active in late August, but this shower needed verification (Jenniskens, 2006). CAMS confirms a weak concentration of radiants in this area. The center of the cluster appears to have a lower perihelion distance than the nearby Northern Piscids.

CAMS does not clearly detect the established Southern ι -Aquiriids (#3, SIA). This shower was identified previously in five photographic surveys from an abundance of low $q = 0.19\text{--}0.36$ AU orbits in the period July 15 to August 25 (Jenniskens, 2006). In CAMS data, orbits with these properties are not distinct from others in the antihelion source at that time.

4.4. The Phaethon Complex

CAMS measured 5103 Geminid orbits, the highest number of any shower (Table 4). There is almost no intrinsic radiant drift after

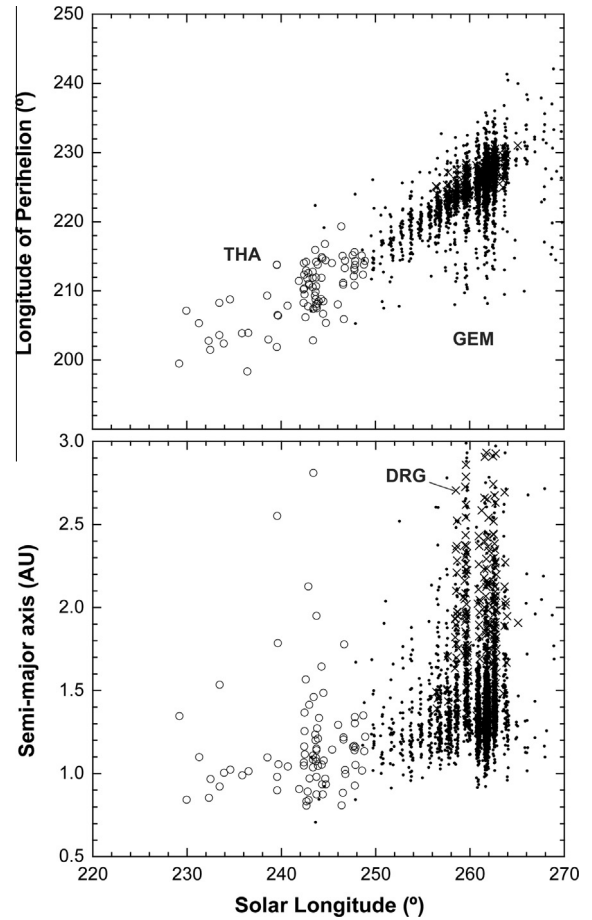


Fig. 11. Geminids – the longitude of perihelion (Π) and the semi-major axis (a) of meteoroid orbits change with solar longitude of the encounter. Open circles are the related θ -Aurigids (THA), while crosses mark the component of fast Geminids here called the December ρ -Geminids (DRG).

correcting for Earth’s motion around the Sun (a least square fits gives -0.12° per degree λ_o). The stream is encountered at a relatively high mean anomaly. The longitude of perihelion changes rapidly along the path of Earth through the stream (Fig. 11), while the argument of perihelion stays nearly constant (not shown). The meteoroids encountered early have a smaller semi-major axis of $a \sim 1.20$ AU at $\lambda_o < 256^\circ$, which increases to $a = 1.32$ AU around the peak. Phaethon has currently $a = 1.271$ AU (Table 4).

The November θ -Aurigids (#390, THA), confirmed in preliminary results published in Jenniskens et al. (2011a), are now even better detected (Fig. 8). They appear to be simply an extension of low- q Geminid orbits toward early November (Table 4). The THA and GEM are continuous in the change of longitude of perihelion (Fig. 11). Late THA have the same $a \sim 1.15$ AU of early Geminids.

Table 4
The Phaethon Complex – the Geminid and Daytime Sextantid showers.

IAU	Object	N	λ_o	R.A.	Dec.	V_g	a	q	e	i	ω	Node	Π	T_J
641	DRG	60	262	113.2	+32.4	39.5	2.12	0.111	0.949	30.9	325.7	261.8	227.3	2.80
4	GEM	5103	262	113.5	+32.3	33.8	1.31	0.145	0.889	22.9	324.3	261.7	225.8	4.41
	*Phaethon	A	261.9	114.3	+33.9	33.9	1.271	0.140	0.889	24.1	325.3	261.9	227.2	4.51
221	DSX	14	188	156.6	-2.4	32.9	1.14	0.147	0.874	24.3	214.3	6.4	219.1	4.97
	*2005 UD	A	189.2	159.9	-3.0	32.9	1.275	0.163	0.872	21.6	217.1	9.2	226.3	4.51
390	THA	82	244	95.7	+34.7	32.5	1.12	0.142	0.879	24.9	327.5	243.6	210.7	5.01
253	CMI	32	252	102.4	+14.5	40.2	1.88	0.074	0.961	29.2	152.5	72.2	225.8	3.00

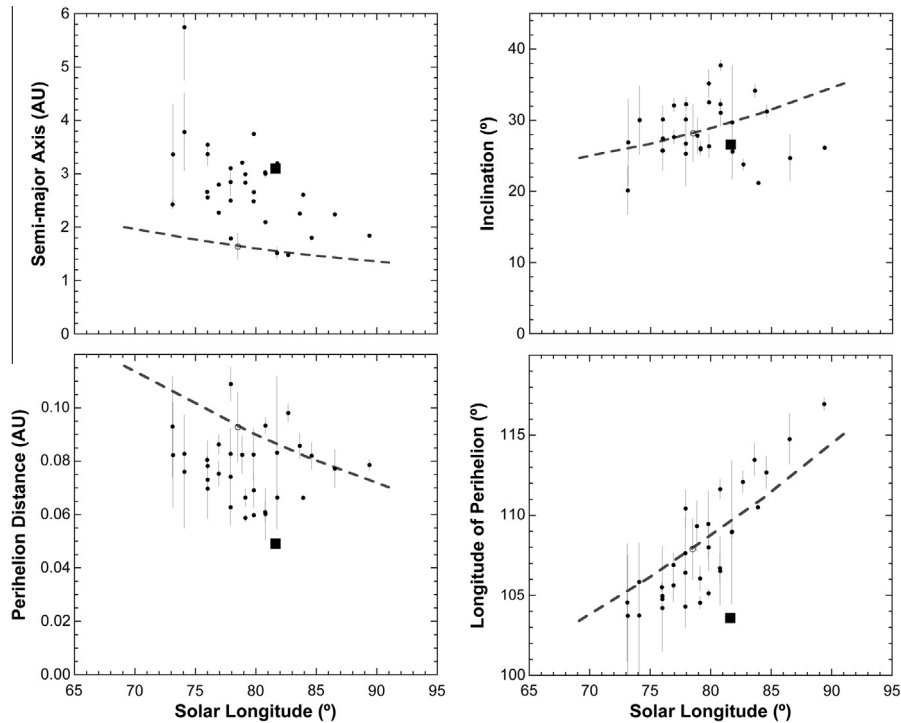


Fig. 12. Daytime Arietids – orbital elements as a function of solar longitude. Data are compared to those of the Marsden sunskirter Comet P/1999 J₆ (solid square) and the reported CMOR radar data (dashed line) from Campbell-Brown (2004).

On the other hand, many THA have a slightly higher argument of perihelion than the Geminids and most were detected in a narrow period centered on $\lambda_o = 243^\circ$ (Fig. 11). The THA are diffuse in inclination and perihelion distance, and are split perhaps into two components, one similar to the Geminids at $i = 21.8^\circ$ and $q = 0.15$ AU, and one at a higher inclination of $i = 27.9^\circ$ and $q = 0.11$ AU.

A possible twin shower of the Geminids was detected south of the ecliptic plane: the December Canis Minorids (#253, CMI), now confirmed (Table 4). The longitude of perihelion is similar to that of the other Phaethon Complex showers, but the semi-major axis is perhaps slightly higher.

As a final curiosity, a group of unusual Geminids was found to have relatively high ~ 39.5 km/s entry speed (7σ above the median 33.8 km/s of other Geminids) and a resulting high $i \sim 28^\circ$ and semi-major axis $a \sim 1.5$ – 3.0 AU (Fig. 11). Based on the medium measurement error, we expected only 3 such outliers. These are here called here the December ρ -Geminids (#641, DRG).

4.5. The Machholz Complex

The Machholz Complex includes 96P/Machholz, the Marsden and Kracht sunskirter comets, as well as several meteoroid streams, which all align along a nutation cycle (Sekanina and Chodas, 2005; Jenniskens, 2006). In this case, the inclination and perihelion distance oscillate with large amplitude while the nodal line rotates. The showers include the Daytime Arietids (#171, ARI), the Southern δ -Aquadriids (#5, SDA), the Quadrantid shower (#10, QUA), the Northern δ -Aquadriids (#26, NDA) and, we now find, also the August ι -Cetids (#505, AIC), first detected by Andreic et al. (2013).

CAMS detected a total of 31 Daytime Arietids in the hours before dawn, with a median semi-major axis for this stream $\langle a \rangle = 2.77 \pm 0.15$ AU (Table 5), dispersed by $\sigma = \pm 0.82$ AU. The shower has a relatively wide activity profile. The strong change of orbital elements with solar longitude noted earlier from CMOR

Table 5
The Machholz Complex – the Daytime Arietids, delta Aquariids, and Quadrantids.

IAU	Object	<i>N</i>	λ_o	R.A.	Dec.	V_g	<i>a</i>	<i>q</i>	<i>e</i>	<i>i</i>	ω	Node	<i>II</i>	<i>T_j</i>
	*96P/Machholz	<i>H</i>	81.9	43.1	+33.6	42.8	3.03	0.124	0.959	56.2	37.5	81.9	109.4	1.94
171	ARI all	31	77	43.9	+24.4	41.1	2.67	0.078	0.974	27.7	28.7	79.1	106.7	2.24
171	ARI center	14	77	44.0	+24.1	41.3	3.13	0.075	0.976	26.6	28.7	76.5	105.2	1.98
	*P/1999 J ₆ (Marsden)	<i>H</i>	80.5	46.6	+23.2	42.8	3.10	0.049	0.984	26.6	23.3	80.5	103.8	1.92
640	AOA = SDA > 132°	316	137	348.5	−14.4	38.2	2.22	0.112	0.950	24.9	146.1	317.0	103.4	2.69
	?P/2000 O3 (Kracht)	<i>A</i>	123.4	337.1	−16.0	42.5	3.04	0.054	0.982	27.6	155.6	303.4	99.0	1.99
5	SDA < 132°	1382	128	341.3	−15.7	41.3	2.59	0.069	0.975	29.0	152.9	306.6	98.9	2.17
	*C/2008 Y12	<i>A</i>	125.4	338.7	−16.4	42.0	3.08	0.065	0.979	28.8	153.1	305.4	98.5	1.98
10	QUA all	1029	283	230.2	+49.5	40.7	2.82	0.979	0.657	71.2	171.4	283.3	94.6	2.19
10	QUA backgr.	163	282	227.8	+51.9	40.3	3.08	0.980	0.683	69.7	177.0	286.4	101.6	2.08
	*2003 EH1	<i>Q</i>	283.0	229.8	+49.5	40.2	2.57	0.979	0.619	70.9	171.4	283.0	94.4	2.07
26	NDA	251	141	347.6	+2.1	38.4	1.97	0.090	0.955	22.3	330.7	140.8	111.1	2.96
505	AIC	64	151	2.0	−7.7	37.7	2.07	0.109	0.948	20.9	145.9	334.4	119.9	2.85
15	URS	62	271	219.9	+75.4	32.9	4.87	0.940	0.807	52.6	205.6	270.1	115.8	1.76
	*8P/Tuttle	<i>Q</i>	270.3	213.4	+74.4	34.3	5.18	0.933	0.820	55.0	207.5	270.3	117.8	1.60

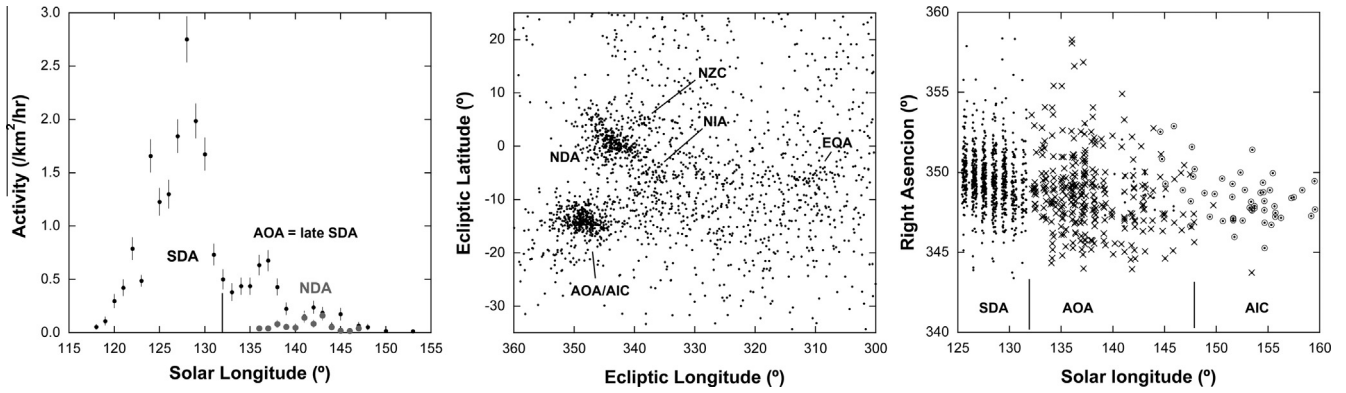


Fig. 13. Southern δ -Aquariids – activity profile (left), radiant in sun-centered ecliptic coordinates (middle) and intrinsic radiant drift (right) for meteors radiating from the Southern δ -Aquariids radiant in August during solar longitudes 132–153°. Shower members in the range $\lambda_o = 132$ –148° are called the August o-Aquariids (AOA), while the late $\lambda_o = 148$ –163° component is the August ι -Cetids (AIC). Other showers shown are the Northern δ -Aquariids (NDA), the ϵ -Aquariids (EQA) = late α -Capricornids, the Northern ι -Aquariids (NIA), and the Northern June Aquilids (NZC).

observations by Campbell-Brown (2004) are confirmed, except that the semi-major axis of our video-derived orbits is systematically higher than that measured by CMOR and the perihelion distance is generally smaller (Fig. 12). In both cases, values are closer to those of Marsden sunskirter Comet P/1999 J₆ (shown as a square dot in Fig. 12). Most interestingly, the deviation of q from this trend (Δq) correlates with the semi-major axis, a larger negative deviation from the CMOR mean line corresponding to the higher semi-major axis values. There is also a good correlation with the longitude of perihelion, more negative values correspond to the lower values of Π (Fig. 12).

Like the Daytime Arietids, the Southern δ -Aquariids too show a relatively wide activity profile. This one is decidedly asymmetric, with higher rates persisting into August (Fig. 13). After $\lambda_o = 132^\circ$, the radiant becomes diffuse. Activity of this late component peaks at $\lambda_o = 137^\circ$, during a gradual shift of the radiant position. The

radiant drift and the drift of orbital elements with solar longitude are discontinuous at this junction (Fig. 14): the late Southern δ -Aquariids after $\lambda_o = 132^\circ$ have less intrinsic radiant drift and a lower semi-major axis. These late SDA are now called the August o-Aquariids (#640, AOA).

The Northern δ -Aquariids (Fig. 13) have a semi-major axis $a = 1.97$ AU on average, smaller than the previous showers, while Π does not follow the trend seen above. Instead, Π is much more similar to that of 96P/Machholz (Table 5). The shower's radiant distribution has a tail to higher Right Ascension and declination (Fig. 13). No associated sunskirter comets have been detected so far.

Following the August o-Aquariids, activity continues at the position of the Southern δ -Aquariids radiant, peaking again in late August centered on $\lambda_o = 154^\circ$. This shower is known as the August ι -Cetids (#505, AIC), and now confirmed (Fig. 13). This shower,

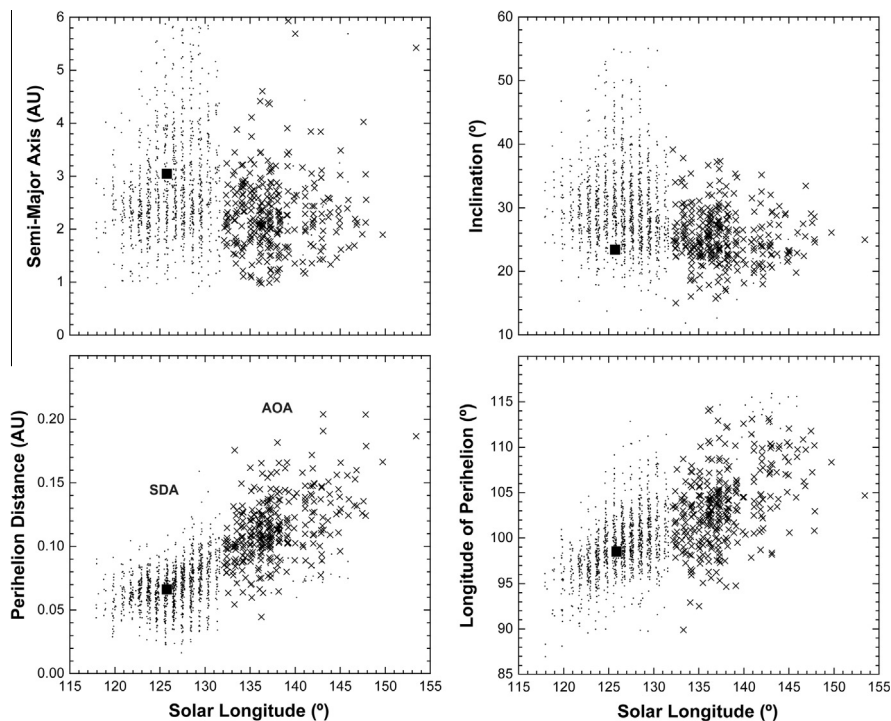


Fig. 14. Southern δ -Aquariids – orbital elements as a function of solar longitude. Elements for Comet C/2008 Y₁₂ are shown as a solid square. Crosses show members of the component called the August o-Aquariids (AOA).

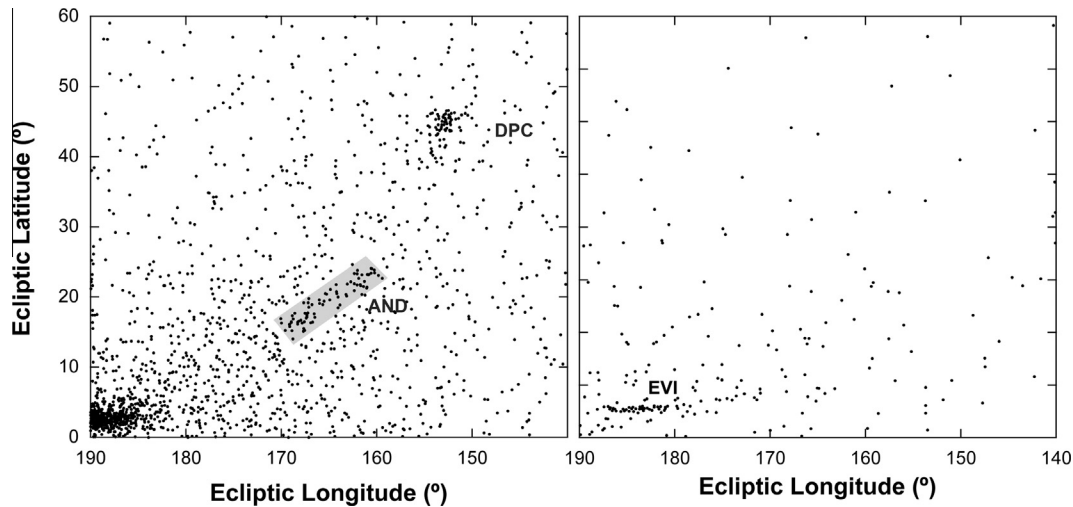


Fig. 15. Andromedids and Eta Virginids – left: Radiants in sun-centered ecliptic coordinates during $\lambda_o = 212\text{--}256^\circ$, showing the annual Andromedids (AND) and the outburst 2011 December ϕ -Cassiopeiids (DPC). The antihelion source is to the bottom left. Right: Same for $\lambda_o = 351\text{--}359^\circ$, with 2013 outburst of η -Virginids (EVI).

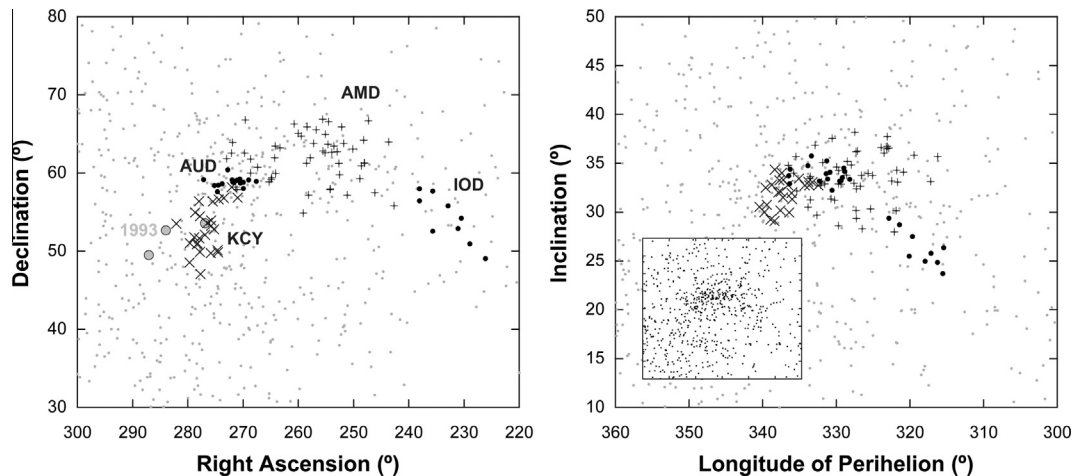


Fig. 16. Kappa Cygnids – sun-centered equatorial radiants (right) and $II-i$ diagram (left, with inset showing unlabeled data) of meteors observed in the period $\lambda_o = 136\text{--}159^\circ$. Symbols mark the κ -Cygnids (KYC), August Draconids (AUD), August μ -Draconids (AMD), and ι -Draconids (IOD). Gray circles show the photographed radiant of outburst 1993 κ -Cygnids (Jenniskens, 2006).

rather than the SDA, appears to be a twin shower of the Northern δ -Aquiriids, representing dust that has continued to evolve along the nutation cycle. The shower has the same low mean semi-major axis ($a = 2.11$ AU) and $II = 119^\circ$. This shower, like the NDA, has no known parent body.

4.6. Established showers from Jupiter-family comets

In recent times, a well observed comet disruption was that of Comet 3D/Biela in about 1842/43 (Marsden and Sekanina, 1971). Today, the annual Andromedids (#18, AND) display an interesting pattern by moving in radiant to higher ecliptic latitudes later in the year, causing the band in Fig. 15 over the period $\lambda_o = 212\text{--}235^\circ$. The shower was most notably present around $\lambda_o = 224^\circ$, but CAMS also detected a concentration of radiants around $\lambda_o = 233^\circ$. On Dec 2–5, 2011, a strong outburst was detected both by CAMS (Jenniskens, 2012; Jenniskens et al., 2012a) and the CMOR radar (Wiegert et al., 2013), and given the name December ϕ -Cassiopeiids (#446, DPC). From December 2 onwards (01:48–14:27 UT), CAMS detected $N = 2, 12, 20, 35, 0$ DPC, respectively. Wiegert et al. (2013) attributed this outburst to past activity from

Comet 3D/Biela, from a time before the comet had been discovered. That makes this outburst distinct from past Andromedid storms and outbursts, which resulted mostly from the post breakup 1846- and 1852-return ejecta, when the comet was seen split in two (Jenniskens and Vaubaillon, 2007). Until now, we have seen no evidence of dust generated during the 1842/43 disruption (Jenniskens and Vaubaillon, 2007). The longitude of perihelion and eccentricity of the orbit do suggest a relationship between DPC and 3D/Biela (Fig. 15, Table 6), but the motion of the DPC radiant during its brief period of activity does not align with that of the annual Andromedids (Fig. 15). So far, no remaining comet fragments were found, but it is not impossible that the DPC originated from one such fragment.

Fig. 15 also shows the η -Virginids (#11, EVI), a strong shower detected during a week in March 2013 ($\lambda_o = 351\text{--}359^\circ$), when from March 11 onwards: 0, 5, 4, 1, 2, 3, 12, 9, and 4 meteors were seen. March 20 was clouded. Cloudy weather in 2011 and 2012 prevented observations on these nights. The shower has an unusual distribution of radiants: narrow in ecliptic latitude but extended in longitude (Fig. 15), suggesting this is recently created debris and the 2013 activity was a meteor outburst (Table 6).

A very complicated situation exists in August, when slow meteors come from Cygnus and Draco (Fig. 16). The whole area shows a diffuse but well-isolated concentration of activity in the Π - i diagram (inset in right diagram of Fig. 16). We de-constructed a series of shower components as follows, but the results may not be unique. We started with the κ -Cygnids (#12, KCY), a shower known from outbursts rich in fireballs around the peak of the Perseids (Jenniskens and Vaubaillon, 2008). In 1993, high numbers of κ -Cygnids were photographed by Dutch Meteor Society observers: 32 meteors clustered at R.A. = 276.9°, Decl. = +53.6°, V_g = 21.4 km/s at λ_o = 140.9° (Table 6), while tight groups of 4 and 5 radiated from nearby positions (gray circles in Fig. 16). A similar outburst did not occur during the CAMS period of observations described here, but SonotaCo data show a κ -Cygnid outburst in 2007, positioned at R. A. = 286.0°, Dec. = +47.8°, with speed V_g = 21.7 km/s at λ_o = 140°, in good agreement. We assigned all similar meteors around this position to shower #12 (Fig. 16).

A group of radiant just above the κ -Cygnid radiant were assigned to the established August Draconids (#197, AUD). After λ_o = 145°, activity jumps to a different position, identified as the August μ -Draconids (#470, AMD), a shower that is now confirmed. In addition to showers KCY (λ_o = 136–143°), AUD (λ_o = 140–145°), and AMD (λ_o = 145–158°), we also identified a nearby shower called the ι -Draconids (#703, IOD) at λ_o = 154–159° (Fig. 16). It is possible that all these showers relate to asteroid 2008 ED₆₉ (Jenniskens and Vaubaillon, 2008) as a product of a disruption cascade. So far, other proposed candidate parent bodies are not a good match (e.g., Jones et al., 2006).

Table 6 lists other established JFC-type showers that were detected by CAMS during the time discussed here. The outburst of October Draconids (#9, DRA) in 2011 was observed from Kuelungsborn and Dunkelsdorf in Germany, where two of the CAMS units (4 cameras each) had been taken to measure meteoroid trajectories. 22 precise trajectories were measured, results of which were published in Jenniskens et al. (2011b). The measured median orbital elements are in good agreement with those expected for dust ejected in 1900 A.D. by parent Comet 21P/Giacobini-Zinner (Table 6). The measured geocentric radiant dispersion (σ = 1.26° in R.A. and 0.98°) is mostly due to measurement error, as the theoretical dispersion is only about $\pm 0.12^\circ$ in R.A. and $\pm 0.05^\circ$. The measured median error was 2.33° in R.A. and

0.71°. Due to clouds, CAMS did not observe the reported DRA outburst in 2012 (Ye et al., 2013).

The highly inclined but very compact γ -Ursae Minorids (#404, GUM) are active at λ_o = 298°, close to but well isolated from the Ursids (#15), which are active earlier in the month around λ_o = 271° (Table 6). Due to weather, all but one meteor was observed in 2013.

The o-Eridanids (#338, OER) are diffuse but well separated from the antihelion source. They are well detected (Jenniskens et al., 2011a). Finally, the established highly inclined and compact x-Herculids (#346, XHE) were only weakly detected.

4.7. The established long-period comet showers

Results for the established Long Period comet (LPC) type showers are listed in Table 7. Such showers tend to have low dust density, diluted on account of a long orbital period. The node of the stream does not change significantly over long periods of time, as a result of which most showers are active only for a few days and have a relatively compact radiant. These showers stand out only in collected data over intervals of $\leq 10^\circ$ solar longitude and typically require a threshold value of $D_{sh} < 0.10$. Most LPC-type shower values for semi-major axis are in the range of a = 10–30 AU. Our values for the meteoroid stream tend to be lower than that of the parent comet. This could be a selection effect, with shorter orbits frequenting Earth more often, or an issue with the initial speed being slightly underestimated in the CAMS observations.

Outbursts from meteoroids on long-period (>250 y) orbits are thought to arise mainly from crossing the 1-revolution dust trail of LPC, because perturbations cause the dust to disperse rapidly in the next return (Jenniskens, 2006). The first reported example of such outburst in CAMS data was a compact cluster of 6 meteors with a high declination and no other activity around (Jenniskens and Gural, 2011). The six meteoroids had identical orbits to within their measurement error and were observed over a period of a few hours on February 4, 2011. The shower now is called the February η -Draconids (#427, FED). No new cases have surfaced since, but such showers are known to happen only once or twice every 60 years for any given comet dust trail that passes to within ± 0.011 AU from Earth's orbit (Lyytinen and Jenniskens, 2003).

Table 6
Jupiter-family comets – established showers with $2.0 \leq T_j < 3.0$.

IAU	Object	N	λ_o	R.A.	Dec.	V_g	a	q	e	i	ω	Node	Π	T_j
18	AND	39	223	20.7	+28.0	18.2	2.99	0.759	0.742	9.4	243.7	222.5	106.8	2.74
446	DPC	68	252	19.5	+57.7	16.5	3.10	0.896	0.714	18.0	218.7	252.1	110.9	2.71
	*3D/Biela (1832)	H	250.7	26.2	+46.3	15.8	3.53	0.879	0.751	13.2	221.6	250.7	112.3	2.53
12	KCY (1993) ^a	25	141	277.5	+52.8	20.9	2.95	0.995	0.662	32.5	196.9	140.0	337.4	2.72
12	KCY (1993) ^a	4	139	284.0	+52.7	24.0	5.12	0.984	0.808	35.9	201.4	139.4	340.8	1.96
12	KCY (1993) ^a	5	140	287.1	+49.5	23.4	4.10	0.957	0.767	34.7	206.2	140.4	346.6	2.21
12	KCY	25	141	277.5	+52.8	20.9	2.95	0.995	0.662	32.5	196.9	140.0	337.4	2.72
197	AUD	17	143	271.7	+58.9	21.1	2.82	1.008	0.644	33.8	188.7	142.6	331.2	2.78
470	AMD	53	149	256.4	+62.5	21.3	2.87	1.009	0.648	33.8	175.5	149.5	327.5	2.75
	*2008 ED ₆₉	P	153.6	246.0	+66.5	22.9	2.89	1.001	0.654	36.4	167.6	153.6	321.2	2.59
703	IOD	12	157	232.3	+53.3	17.8	2.93	0.990	0.664	26.1	161.5	157.2	318.8	2.78
9	DRA (2011)	30	195	262.9	+55.7	20.7	3.15	0.996	0.706	31.4	173.2	195.0	8.3	2.51
	*21P/G.-Z. (1900)	- ^b	195.0	263.2	+55.8	20.9	3.47	0.996	0.707	31.8	173.5	195.0	8.5	2.46
11	EVI (2013)	56	357	184.8	+3.9	26.6	2.47	0.460	0.812	5.4	281.0	355.7	277.4	2.91
	?2003 FB5	W	358.4	188.8	+1.8	26.7	2.52	0.532	0.789	5.4	273.2	358.4	271.6	2.92
63	COR	12	86	205.8	+0.2	8.7	2.35	0.999	0.571	2.6	193.7	91.8	284.2	3.32
	?2008 OY2	H	90	202.7	-5.6	8.8	2.65	1.006	0.620	0.9	193.4	90.0	283.4	3.09
404	GUM	26	298	228.3	+69.2	28.8	2.88	0.952	0.671	47.1	203.4	298.8	142.4	2.56
346	XHE	5	350	253.0	+49.2	35.2	2.99	0.975	0.673	59.8	196.7	350.0	186.5	2.30
338	OER	69	232	59.9	+0.1	28.5	3.92	0.497	0.875	19.6	94.1	49.2	141.9	2.12

^a Photographic observations during the 1993 KCY outburst (Jenniskens and Vaubaillon, 2008).

^b Radiant and peak time from meteoroid stream modeling (Vaubaillon et al., 2011).

Annual shower components, representing dust from at least 2 revolutions old (Jenniskens, 2006), are sometimes detected also from LPC-type orbits. The Lyrids (#6, LYR) from Comet C/1861 G₁ (Thatcher) are active over six days ($\lambda_o = 29\text{--}34^\circ$) and are well isolated from the sporadic background. This comet moves in a ~ 415 -y orbit, short as far as long-period comets go (Jenniskens, 2006). Curiously, the radiant is slightly more diffuse outside the core period of stream activity at $\lambda_o = 32\text{--}33^\circ$.

The Aurigids (#206, AUR) from Comet C/1911 N₁ (Kieess) show a compact slightly elongated radiant, active over 6 days also. Most meteors were detected in 2011. The shower is known for periodic outbursts.

Eight out of nine selected October Ursae Majorids (#333, OCU) are from the night of October 15, 2012. Good data at that solar longitude existed also from 2011, which implies that the activity is not annual and this shower had an outburst in 2012.

Good detections were made also of the Leonis Minorids (#22, LMI), the η -Lyrids (#145, ELY), and the κ -Ursae Majorids (#445, KUM). The KUM are known for outbursts. Five out of 8 KUM were detected in 2012, but over a 3-day period and with significant dispersion in radiant positions, suggesting CAMS-detected activity was annual in nature.

Some showers have a relatively long duration. The strong December Monocerotids (#19, MON) from Comet C/1971 F₁ (Melish) show some sign of substructure, but not conclusively enough to extract components. Good detections were made also of the compact ε -Geminids (#23, EGE), which does appear to have a long orbital period. The strong July γ -Draconids (#184, GDR) show an intrinsically drifting radiant to lower ecliptic longitude later in the month (Holman and Jenniskens, 2012b). The July Pegasids (#175, JPE) have a compact radiant too, but a large spread in entry speed, with a changing longitude of perihelion from $\Pi = 354^\circ$ to 28° during the time of the observations, possibly extending to $\Pi = 65^\circ$ in late July. The orbital period of the meteors suggests that this dust is from a long-period comet also.

4.8. A Halley Complex?

Comet 1P/Halley, the poster child of Halley-type comets (HTC), is responsible for the Orionids (#8, ORI) and η -Aquariids (#31, ETA). The first CAMS observations were made during a predicted outburst of Orionids on October 21, 2010 (Sato and Watanabe, 2007; Jenniskens et al., 2010a). These outbursts are thought to be

caused by dust trapped in the 6:1 mean-motion resonance with Jupiter at $P = 71$ yr (Sekhar and Asher, 2014). A compact radiant would be expected. 38 Orionid trajectories were measured that night, 21 with an error better than $\pm 0.4^\circ$ in radiant (Fig. 17). Results for the 14 meteors near the center of the image are given separately in Table 8. The accuracy of the semi-major axis ($a = 10\text{--}28$ AU, $\langle a \rangle = 11.7$ AU) is not enough to identify the mean motion resonance with Jupiter that traps the dust. The median value is slightly higher than that of annual Orionids, and closer to that of 1P/Halley itself.

A similar outburst component is sometimes observed in activity of the η -Aquariids (#31, ETA) in the range of $\lambda_o = 45\text{--}47^\circ$ (Jenniskens, 2006). CAMS data show a compact radiant on those dates. Results from 41 meteors are given separately in Table 8, again showing a semi-major axis slightly higher than that of the annual ETA.

Are these the only showers related to Comet 1P/Halley? A striking feature in Fig. 1 is the tail of activity that extends from the Orionid radiant to southern latitudes (see arrow in left diagram). This area is enlarged in Fig. 18. These showers stretch over the months of August to November and this “Orionid tail” is not obvious before radiant drift correction (Fig. 18, left side). The tail is first detected when the η -Eridanids (#191, ERI) activity ends at around $\lambda_o = 152^\circ$ in late August. This shower has a very long activity period from $\lambda_o = 117^\circ$ to 152° .

Some individual components of the Orionid tail were recognized in previous meteoroid orbit surveys. Leading up to the Orionids, there is first the compact 27-Monocerotids (#558, TSM), only recently proposed from Croatia Video Network and SonotaCo data by Andreic et al. (2014) and now confirmed (Fig. 18). The number 27 refers to the Flamsteed number of the star in the naming. In the drift uncorrected radiant data, TSM is well separated from the other showers. Next are the σ -Orionids (#225, SOR), now confirmed, followed by the established ν -Eridanids (#337, NUE). The SOR are later than the NUE in activity and extend from $\lambda_o = 188^\circ$ to 208° . Next are the September o-Orionids (#479, SOO), now confirmed, and the newly named ξ -Geminids (#718, XGM).

What appear to be unrelated showers, but located close to the tail in sun-centered coordinates (Fig. 18), are the diffuse π^6 -Orionids (#552, PSO), now confirmed, and two newly identified showers, the λ -Geminids (#719, LGM) and the ρ -Eridanids (#738, RER). The PSO represent a complex distribution of meteoroid orbits and distribute strangely in the uncorrected

Table 7
Long Period comets – established showers with $T_J < 2.0$.

IAU	Object	<i>N</i>	λ_o	R.A.	Dec.	V_g	<i>a</i>	<i>q</i>	<i>e</i>	<i>i</i>	ω	Node	Π	T_J
6	LYR	258	32	272.0	+33.4	46.7	10.8	0.921	0.956	79.4	214.0	32.3	246.1	0.47
	*1861 G1	Q	31.9	272.0	+33.5	47.1	55.7	0.923	0.984	79.8	213.5	31.9	245.4	0.30
22	LMI	64	209	159.9	+36.6	61.9	10.6	0.620	0.989	125.2	104.3	208.2	313.4	-0.46
	*1739 K1	Q	211.0	162.6	+36.2	61.9	Inf.	0.624	1.000	124.3	104.8	211.0	315.8	-0.57
23	EGE	31	198	93.8	+28.1	69.6	11.3	0.813	0.957	171.2	230.9	198.4	68.8	-0.79
145	ELY	39	49	289.9	+43.4	43.7	21.4	0.999	0.954	74.1	192.3	50.1	242.7	0.58
	*1983 H1	Q	49.1	288.4	+44.0	43.8	98.1	0.997	0.990	73.3	192.9	49.1	241.0	0.41
175	JPE	104	108	347.2	+10.0	64.0	7.26	0.562	0.960	149.2	265.0	112.4	20.9	-0.38
	*1979 Y1	H	110.5	348.5	+10.5	64.1	45.3	0.545	0.988	148.9	266.2	110.5	16.7	-0.66
	?1771 A1	H	118.2	354.8	+13.2	64.1	Inf.	0.528	1.000	148.8	267.7	118.2	25.9	-0.77
184	GDR	40	124	280.1	+50.3	27.5	16.4	0.977	0.967	40.3	202.5	124.7	327.4	1.10
206	AUR	19	158	90.9	+38.6	65.6	13.2	0.663	0.956	149.1	107.3	156.2	263.9	-0.53
	*1911 N1	Q	158.7	91.4	+39.2	66.1	184.1	0.681	0.996	148.4	110.4	158.7	269.1	-0.84
246	AMO ^a	10	239	116.8	+0.9	63.0	500	0.488	0.999	134.1	90.7	59.3	150.0	-0.59
333	OCU	9	202	145.0	+64.8	55.6	12.6	0.982	0.967	100.6	165.9	202.2	8.2	-0.05
19	MON	249	261	102.9	+7.8	41.4	8.20	0.191	0.983	35.2	128.7	78.5	207.4	0.90
	*C/1917 F1	H	262.8	103.7	+8.8	41.5	27.6	0.190	0.993	32.5	128.3	82.8	211.1	0.64
427	FED	9	315	239.6	+62.4	35.1	18.6	0.971	0.975	54.7	194.3	315.1	149.3	0.84
445	KUM	8	225	147.2	+45.0	65.7	Inf.	0.988	1.000	129.6	185.9	224.0	50.7	-0.01

^a From photographic orbits during meteor outbursts (Jenniskens et al., 1997).

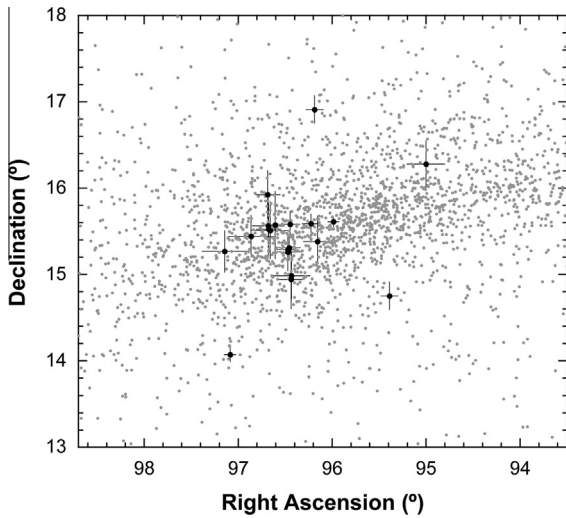


Fig. 17. Orionids – radiant distribution in sun-centered equatorial coordinates of all extracted Orionids, and drift corrected to $\lambda_o = 209^\circ$, where black dots are the precisely measured Orionids (with angular errors $<0.5^\circ$) from the outburst night of October 21, 2010.

radiant diagram. More data is needed to sort out if more than one shower is responsible. The previously reported October Monocerotids (#227, OMO) are said to be located just below shower #225 (Jenniskens, 2006), but were not detected.

All showers in the “Orionid tail” are listed in Table 8. They have Halley-type semi-major axis $a = 5\text{--}12$ and show a wide range in longitude of perihelion, with a general trend of increasing Π with solar longitude. The relation of these showers to Comet 1P/Halley, if any, needs study.

4.9. The established Halley-type showers

Halley-type comets (HTC) are rare, but their dust ejecta can get trapped in mean-motion resonances, resulting in accumulations that can persist even when the comet orbit has precessed away from Earth’s orbit (Jenniskens, 2006). As a result, many HTC type showers exist that have parent bodies in now quite different orbits. Orbital elements for the remaining Halley-type showers in the IAU Working List are summarized in Table 9, which gives retrograde orbits related to the apex sources, Table 10 that has high inclination prograde orbits related to the toroidal complex, and in Table 11 that has paired showers of HTC and JFC type.

The large 26-km diameter Halley-type Comet 109P/Swift–Tuttle is the parent body of the Perseid shower (#7, PER). The shower has a well-defined radiant position after drift correction. In the solar longitude interval $\lambda_o = 105\text{--}114^\circ$, another component is located close to it in sun-centered coordinates (Zoladek and Wisniewski, 2012; Segon et al., 2012), now called the ζ -Cassiopeiids (#444, ZCS). This shower may also originate from 109P/Swift–Tuttle. The longitude of perihelion is lower ($\Pi = 278^\circ$ versus 292°), but this fits in a trend of changing Π versus solar longitude.

The annual Leonids (#13, LEO) of Comet 55P/Tempel–Tuttle are well detected. The radiant gradually moves to lower ecliptic longitude and the combined radiant has a faint tail in that direction.

The January Leonids (#319, JLE), first detected in the CMOR survey (Brown et al., 2010), holds the record for the lowest median perihelion distance. The shower has $q = 0.048 \pm 0.007$ AU. Thirteen shower members were observed, all in the period 2011 December 31–2012 January 7. This may have been an outburst.

The σ -Hydrusids (#16, HYD) show a relatively large dispersion in longitude of perihelion and inclination and contain a late diffuse component. A compact group of 8 HYD were detected in 2011 with higher perihelion distances, perhaps a meteor outburst. Because the parent body is unknown, this object may at present be a high impact risk to Earth. Other detected retrograde showers listed in Table 9 include the ψ -Ursae Majorids (#339, PSU) in a short $\Delta\lambda_o = 10^\circ$ window, the strong ϕ -Piscids (#372, PPS), and the strong c-Andromedids (#411, CAN) (Holman and Jenniskens, 2013). The strong December χ -Virginids (#335, XVI) are detected over a wide 34° interval.

The Comae Berenicids (#20, COM) are active in December and January over a long time interval. The shower was previously known as the December Leonis Minorids, before the IAU Task Group on Meteor Shower Nomenclature adopted the name Comae Berenicids. After drift correction, the radiant is compact but elongated in ecliptic longitude and has a tail to lower ecliptic longitude. Several previously identified showers were mere parts of this stream. No individual components are found, except for the late February η -Virginids (#506, FEV) (Steakley and Jenniskens, 2013). This shower, too, has a high semi-major axis, suggesting that a massive long-period comet is responsible. No parent body is known.

The September ϵ -Perseids (#208, SPE) were detected over a relatively long interval between $\lambda_o = 161^\circ$ and 190° with a similar rate profile in 2011 and 2012, in both years having highest rates during a narrow 5° wide peak centered on 167.0° . The shower is known for its 2–4 h wide outbursts in 2008 and 2013, at

Table 8
The Halley Complex – includes showers in the “Orionid tail” in order of solar longitude.

IAU	Object	N	λ_o	R.A.	Dec.	V_g	a	q	e	i	ω	Node	Π	T_j
31	ETA 45–47°	41	47	339.2	−0.3	65.5	10.3	0.576	0.944	163.5	96.7	46.2	142.9	−0.39
31	ETA	936	46	338.1	−0.8	65.7	7.41	0.587	0.955	163.6	98.4	46.2	144.9	−0.49
	*1P	H	46.1	338.2	−0.3	65.9	17.9	0.586	0.967	162.7	98.5	46.2	144.7	−0.61
191	ERI	214	137	43.7	−11.9	64.5	10.3	0.953	0.945	132.7	28.4	317.7	343.0	−0.51
738	RER	24	137	44.8	−4.0	67.3	8.94	0.988	0.945	145.7	18.7	316.7	335.3	−0.71
337	NUE	291	163	61.5	+4.3	67.1	7.04	0.867	0.916	150.7	43.7	53.2	43.2	−0.47
552	PSO	99	159	70.5	−2.3	65.8	7.53	1.004	0.893	138.3	17.2	342.4	341.5	−0.35
225	SOR	40	187	87.9	+0.5	66.2	9.70	0.934	0.919	139.7	30.6	9.6	40.6	−0.42
479	SOO	40	187	80.9	+12.5	67.6	8.11	0.777	0.911	159.9	57.6	7.7	65.2	−0.41
718	XGM	33	206	96.9	+12.7	68.1	5.78	0.726	0.952	159.9	60.8	26.3	85.6	−0.69
8	ORI (2010)	14	208	95.3	+15.5	66.5	11.7	0.594	0.949	163.5	80.1	27.7	107.8	−0.46
8	ORI	3024	209	95.9	+15.7	66.3	6.87	0.578	0.944	163.9	82.2	28.3	111.0	−0.38
	*1P	H	208.9	96.0	+16.0	66.8	17.9	0.586	0.967	164.6	80.6	28.9	109.5	−0.61
558	TSM	7	227	121.8	−5.8	64.6	6.27	0.899	0.858	134.4	37.4	46.6	83.9	0.04
719	LGM	11	232	106.8	+17.5	60.6	4.68	0.220	0.981	164.7	128.1	52.2	176.9	−0.01

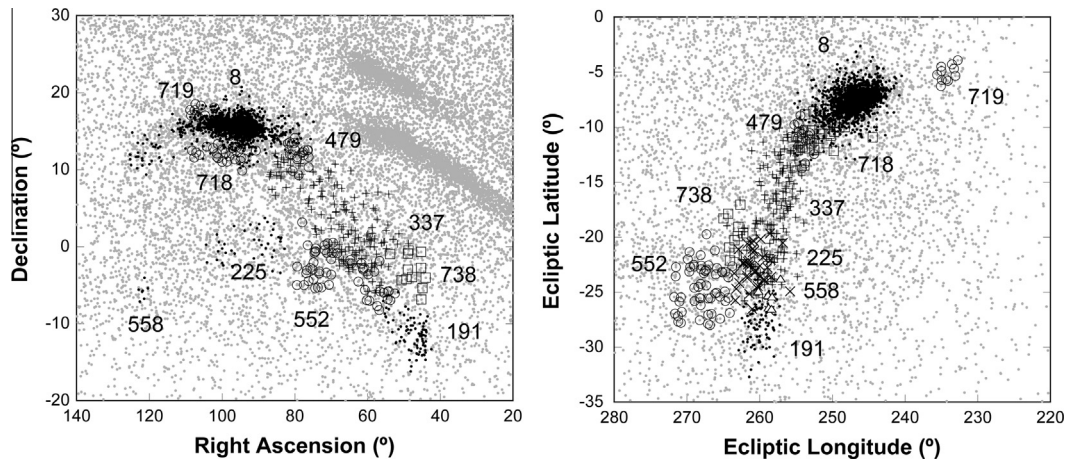


Fig. 18. Orionids – radiant map of showers in the Orion “tail” during the period $\lambda_0 = 137\text{--}239^\circ$, in observed geocentric coordinates (left) and in sun-centered ecliptic coordinates after correcting for radiant drift from Earth’s motion around the Sun (right). Individual showers are shown by different symbols and marked with the IAU assigned shower number.

$\lambda_0 = 166.91^\circ$ and 167.19° , respectively (Gajdos et al., 2014). The long duration of the shower suggests a Halley-type origin.

Among the prograde Halley-type showers are the χ -Taurids (#338, CTA), the α -Hydrids (#331, AHY), the κ -Serpentids (#27, KSE), and the strong November Orionids (#250, NOO), which drift to lower ecliptic longitude (Fig. 7) and are located on the toroidal ring.

Other low- q showers were more difficult to detect. We assigned some meteors in an arc below the reported radiant position to the

α -Antiliids (#110, AAN), but no meteors are extracted starting from the published orbit. Starting from the CMOR-derived orbit (Brown et al., 2010), small numbers of meteors were assigned to the σ -Serpentids (#330, SSE), ϵ -Perseids (#324, EPR) and daytime σ -Serpentids (#320, OSE).

The highly inclined ψ -Cassiopeiids (#187, PCA) are a weak shower, best recognized in the Π - i diagram. The period of activity $\lambda_0 = 103\text{--}128^\circ$ is in good agreement with that of CMOR derived range ($100\text{--}129^\circ$), but we later added some meteors in the

Table 9
Halley-type comets – retrograde showers with $T_J < 1.0$.

IAU	Object	N	λ_0	R.A.	Dec.	V_g	a	q	e	i	ω	Node	Π	T_J
411	CAN	169	107	29.1	+47.3	57.5	8.40	0.687	0.938	112.9	109.1	107.4	215.2	0.07
444	ZCS	118	109	3.1	+49.5	57.1	12.8	1.000	0.962	106.6	165.4	112.1	277.2	-0.16
7	PER	4367	140	48.2	+58.1	59.1	9.57	0.949	0.950	113.1	150.4	139.3	288.7	-0.19
	*109P	H	139.4	45.8	+57.7	59.4	26.1	0.959	0.963	113.5	153.0	139.4	292.4	-0.28
13	LEO	268	235	153.8	+21.8	70.2	6.63	0.983	0.867	162.2	170.8	234.5	45.2	-0.42
	*55P	P	235.0	153.4	+21.8	70.6	10.3	0.984	0.905	162.5	172.2	235.0	47.2	-0.64
16	HYD	528	266	134.4	-0.1	58.9	9.08	0.257	0.985	128.7	119.5	76.5	195.8	-0.08
16	HYD cluster	8	252	123.1	+2.1	60.4	201	0.312	0.998	131.4	111.4	71.7	182.9	0.55
20	COM	497	274	167.0	+28.0	63.3	8.58	0.557	0.962	135.3	263.5	272.2	176.6	-0.29
506	FEV	55	314	200.4	+11.0	62.9	8.28	0.491	0.954	138.0	272.5	312.6	224.6	-0.14
208	SPE	85	168	48.6	+39.6	64.8	8.81	0.718	0.979	139.9	245.3	168.2	54.7	-0.62
319	JLE	13	283	147.7	+24.1	51.4	5.43	0.048	0.991	100.1	335.7	283.4	259.3	0.88
335	XVI	46	267	194.3	-12.0	69.1	6.24	0.663	0.985	169.1	290.3	86.5	24.9	-0.83
339	PSU	18	253	169.8	+42.4	61.7	9.13	0.928	0.901	119.4	208.9	253.8	103.1	-0.02
372	PPS	379	103	17.0	+25.0	66.5	6.63	0.889	0.882	150.4	136.9	102.9	240.7	-0.29

Table 10
Halley-type comets – prograde showers with $0.0 < T_J < 2.0$.

IAU	Object	N	λ_0	R.A.	Dec.	V_g	a	q	e	i	ω	Node	Π	T_J
27	KSE	21	20	240.2	+16.8	46.7	7.90	0.489	0.971	72.5	273.4	20.1	292.1	0.58
110	AAN	34	312	157.2	-9.5	45.0	3.57	0.143	0.965	58.6	138.3	133.4	272.1	1.64
187	PCA	36	119	36.8	+72.2	42.0	4.07	0.829	0.802	74.0	125.0	119.3	245.3	1.50
250	NOO	369	247	90.6	+15.2	42.5	8.36	0.116	0.990	24.4	140.4	67.6	207.8	0.83
320	OSE	2	176	157.3	+27.3	45.0	15.7	0.151	0.990	50.3	45.4	278.7	324.1	0.66
323	XCB	26	296	250.9	+29.7	45.1	4.25	0.784	0.812	78.0	122.7	296.1	59.3	1.44
324	EPR	4	88	53.8	+37.8	43.8	9.05	0.167	0.982	53.0	46.8	87.9	134.8	0.88
330	SSE	3	276	245.4	-4.8	45.5	4.30	0.123	0.972	60.0	39.1	273.3	311.3	1.43
331	AHY	119	284	126.9	-8.7	43.3	7.07	0.297	0.971	58.1	114.6	103.2	217.3	0.85
388	CTA	52	221	63.0	+26.2	41.1	4.76	0.100	0.980	15.0	324.7	220.9	191.2	1.40

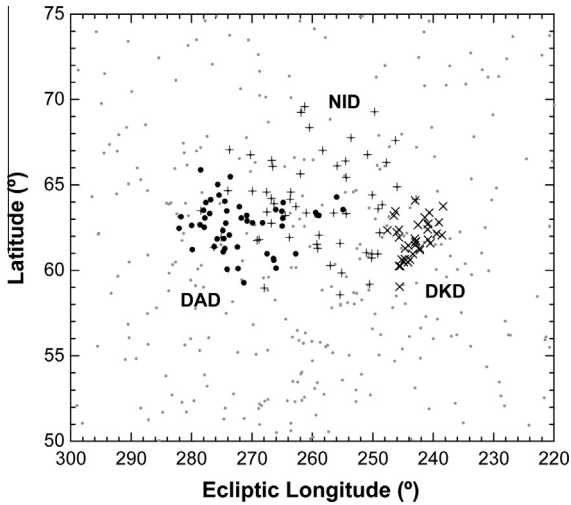


Fig. 19. November i-Draconids – sun-centered ecliptic radiant coordinates in the period $\lambda_o = 247\text{--}269^\circ$, with different symbols marking meteors assigned to the December α -Draconids (DAD), December κ -Draconids (DKD), and November i-Draconids (NID).

125–135° interval. The meteors assigned to these established showers are identified in the CAMS Meteoroid Orbit Database 2.0.

4.10. Paired JFC and HTC showers in the toroidal source

Fig. 19 shows the short-period $a = 2.48$ AU (Table 6) December α -Draconids (#334, DAD), which peak at $\lambda_o = 256.5$ in SonotaCo data (Kanamori, 2009). The nearby December κ -Draconids (#336, DKD) peak just a few days earlier at $\lambda_o = 250.2$ (Kanamori, 2009) but have a Halley-type $a = 10.5$ AU orbit (Table 6). Brown et al. (2010) added a November i-Draconids (#392, NID) at $\lambda_o = 241.0^\circ$, which appears to be a combination of the two previous showers. However, when extracting the DAD and DKD from the sporadic background, we were left with an excess of meteors that did not seem to belong to either the DAD or DKD. These were assigned to shower #392, instead (Fig. 15).

The same combination of HTC- and JFC-type orbits is seen elsewhere in the toroidal ring. The Northern June Aquilids (#164, NZC) and the Southern June Aquilids (#165, SZC) are strong JFC-type showers with high eccentricity, but low semi-major axis, active from June until early August (Table 11). In late July and early August, the Northern June Aquilids are found just above the emerging Northern δ -Aquiriid radiant (Fig. 13) (Holman and Jenniskens, 2012a). Both showers are more diffuse and have lower semi-major axis than the Southern δ -Aquiriids. The showers appear to be twins, suggesting that dust has distributed significantly along the

nutration cycle. Activity is stationary in ecliptic coordinates, but extended to higher ecliptic longitude and latitude early in the activity period. The rate of the more active Northern June Aquilids varies from day to day more than that of other showers during this time, suggesting there may be more than one component. However, the intrinsic radiant drift is too small to be able to extract separate components like we did for the Taurids in Section 4.2. The Halley-type Piscis Austrinids (#183, PAU) are perhaps related (Table 6). This shower does not peak around $\lambda_o = 124^\circ$, as concluded from sparse photographic orbits (Jenniskens, 2006), but ranges from $\lambda_o = 125^\circ$ to 145° instead.

Also in the toroidal source are the January ξ -Ursae Majorids (#341, XUM). XUM with $\Pi = 242\text{--}248^\circ$ have JFC-like Tisserand parameter $T_j = 2\text{--}3$, while those with $\Pi = 248\text{--}254^\circ$ have asteroidal $T_j = 3\text{--}4$ AU. The α -Lyncids (#252, ALY) have the same radiant when corrected for radiant drift, but they have $\Pi = 217^\circ$ and are encountered 31° earlier in solar longitude. A 1971 outburst at solar longitude 268° gives credence to that this shower does exist (Jenniskens, 2006). The only three meteors assigned to this shower have a relatively low semi-major axis $a = 3.6\text{--}13.3$ AU, indicative of a Halley-comet source rather than a Long Period comet (Table 6).

Finally, the HTC-type April ρ -Cygnids (#348, ARC) are at a slightly lower inclination than the JFC-type ν -Cygnids (#409, NCY), showing a jump in activity that justifies assigning two meteor shower names (Jenniskens and Haberman, 2013). Based on overlap in radiant position and speed during the relevant epoch, the ν -Cygnids are the same shower as the ζ -Cygnids (#40, ZCY), an earlier identified shower. Therefore, the ν -Cygnids should be removed from the Working List and the name ζ -Cygnids be used instead.

4.11. Short semi-major axis streams in the toroidal source

A few unusual short semi-major axis ($T_j \gg 3$) showers are included in the IAU List of Established Showers (Table 12), all first reported from radar observations (Sekanina, 1976; Brown et al., 2010). The high Tisserand parameter suggests these originated from disrupted asteroids, but they all have a high inclination and are part of the toroidal source. There is no associated surface density enhancement in the CAMS-detected radiant distribution. Assuming that the showers do exist, we continued to search for associated meteoroids using the D_h criterion starting from the CMOR-reported orbit.

The β -Equuleids (#327, BEQ), with $T_j = 5.1$, have a JFC-like eccentricity but short semi-major axis of $a = 1.03$ AU, with CMOR measuring an even lower $a = 0.89$ AU. This stream stands out well in the distribution of Tisserand parameter with solar longitude. After extracting the stream from this diagram, a diffuse radiant is found just above the Northern June Aquilids (NZC).

Table 11
Toroidal shower complexes – possibly paired showers in the toroidal ring.

IAU	Object	<i>N</i>	λ_o	R.A.	Dec.	V_g	<i>a</i>	<i>q</i>	<i>e</i>	<i>i</i>	ω	Node	Π	T_j
40	ZCY	64	32	309.5	+42.5	43.0	3.93	0.900	0.780	74.9	140.5	31.5	168.9	1.57
348	ARC	42	38	322.1	+46.6	40.9	6.14	0.842	0.864	69.7	130.3	39.4	169.6	1.23
164	NZC	404	101	309.7	−5.3	38.3	1.79	0.114	0.937	38.8	326.9	101.7	67.7	3.21
165	SZC	89	104	319.3	−27.6	39.2	2.00	0.105	0.952	36.1	148.2	282.8	71.7	2.85
183	PAU	23	136	352.5	−20.5	43.8	5.66	0.135	0.980	53.1	139.1	315.3	94.9	1.07
336	DKD	36	252	187.2	+70.2	43.8	10.31	0.929	0.914	73.1	208.5	251.5	100.0	0.82
392	NID	65	242	196.5	+68.0	41.9	3.62	0.973	0.734	72.9	194.7	254.4	87.8	1.77
334	DAD	47	256	210.8	+58.6	40.8	2.48	0.983	0.603	71.8	177.4	254.8	74.2	2.45
341	XUM	30	298	168.7	+33.0	40.9	1.50	0.217	0.857	66.8	313.2	298.0	251.6	3.69
252	ALY	3	272	140.4	+39.8	49.5	6.78	0.213	0.969	84.0	306.4	272.2	217.0	0.83

The ε -Pegasids (#326, EPG), with $T_j = 7.4$ and with $a = 0.73$ AU, have the lowest semi-major axis among established meteor showers. CMOR measured $a = 0.76$ AU, in good agreement. We have a narrow cluster in the II - i diagram, but a wide dispersion in Right Ascension. It is not possible to set a reliable D-criterion threshold.

The ε -Aquilids (#151, EAU), with $T_j = 6.7$ and $a = 0.82$ AU, is at best a weak shower in CAMS data. Sekanina (1976) measured $a = 0.87$ AU, in good agreement.

Finally, the α -Lacertids (#328, ALA) have a median Tisserand parameter $T_j = 5.1$ and $e \sim 0$. These meteors used to be called the “Cyclids”, meteoroids that move in near circular orbits similar to Earth’s orbit (Teren’teva, 1973). Brown et al. (2010) and Sekanina (1976) disagree about the median orbit. Using Sekanina’s orbit, only two meteoroids were detected for $D_d < 0.17$ (Table 12). Only 210 orbits in the CAMS database have $e < 0.10$, which all have $0.81 < q < 1.02$ and $0.90 < a < 1.13$. CAMS data cannot confirm that these two meteoroids originate from the same parent body.

5. Discussion

5.1. Nature of the second α -Capricornid component

In models of dust ejected from 169P/NEAT up to 5000 years ago, Jenniskens and Vaubaillon (2010) found that two strands of dust intersected Earth orbit. One strand corresponds closely in radiant and speed with the observed main peak of the α -Capricornids. In the model, this component has also the highest number of Earth approaching meteoroids. The second strand has a 1.6° higher R.A. and 2.5% higher entry speed ($\Delta V_g = 0.57 \pm 0.02$). The observed second component is 2.6° higher in Right Ascension after correcting the radiant drift to a common solar longitude $\lambda_o = 124^\circ$. The observed entry speed is 7.0% higher ($\Delta V_g = 1.60 \pm 0.08$ km/s, the uncertainty marking the precision of determining the mean, not the $1\text{-}\sigma$ dispersion).

The origin of the second strand in the model is possibly related to the nearby 3:1 mean-motion resonance with Jupiter (Fig. 5c). It is not seen among the smallest meteoroids that are ejected in the highest semi-major axis orbits due to radiation pressure. Parent 169P/NEAT has a semi-major axis $a = 2.6042$ AU (at the 2007-Apr-11.0 ET epoch), just above the 3:1 resonance at 2.52 AU. The main component has an observed semi-major axis of $\langle a \rangle = 2.54 \pm 0.01$ AU. The second component has a smaller $\langle a \rangle = 2.40 \pm 0.02$ AU (Fig. 5). If the actual main-component scatters at or just above the semi-major axis of the comet itself, then the second component would have $\langle a \rangle \geq 2.46 \pm 0.02$ AU, consistent with these meteoroids being trapped in the 3:1 mean-motion resonance.

In detail, however, the secondary component was predicted to be more dispersed in solar longitude and to peak $\lambda_o = 2^\circ$ later than the main component, not 7° earlier. It is also likely that dust trapped in mean-motion resonances would not annually return at the same rate. Instead, we detected the same 47 ± 7 XCS in 2011 as the 39 ± 6 in 2012.

An alternative possibility, and perhaps more likely, is that the ξ^2 -Capricornids originated from a disruption that left the small $D = 100$ -m diameter Comet 2003 T₁₂ (SOHO), recently identified

as a possible fragment from 169P/NEAT (Sosa and Fernández, 2015). Using the method “A” of Neslusan et al. (1998) to calculate the radiant, meaning that the comet orbit is adjusted by a rotation around the line of apsides, shows that meteoroids from 2003 T₁₂ are expected to arrive $\Delta\lambda_o = 3.9^\circ$ earlier in solar longitude and, after correcting for the daily radiant drift to a common solar longitude of $\lambda_o = 124^\circ$, to appear $\Delta\text{R.A.} = 2.0^\circ$ higher in Right Ascension than meteoroids from 169P/NEAT (Table 1). The observed ξ^2 -Capricornids peak $\Delta\lambda_o = 7 \pm 1^\circ$ earlier from a direction $\Delta\text{R.A.} = 2.6 \pm 0.2^\circ$ higher. Both differences are slightly larger than calculated, but in the correct orientation. 2003 T₁₂ may sample just one pathway in the dynamical evolution of the second strand.

If so, that would make these streams a 169P/NEAT Complex, perhaps with the weak and dispersed ε -Aquilids (#692, EQA) component dating from the time of the original disruption that separated 2003 T₁₂ from 169P/NEAT.

5.2. Nature of the Encke Complex showers

Whipple (1940) first proposed that Comet 2P/Encke is the parent body of the Taurid showers. Precession causes a rotation of the nodal line, explaining why the current orbit of 2P/Encke does not pass close to Earth’s orbit. Differences in the rate of precession will disperse the ascending and descending node of the meteoroid orbits along the ellipse of the comet orbit, resulting in Northern and Southern Taurid branches above and below the orbital plane of Jupiter where they intersect Earth’s orbit arriving from the night side. One rotation of the nodal line takes about 5900 yr.

Precession will also gradually rotate the longitude of perihelion II . The core Taurids are dispersed by 45° ($II = 125\text{--}170^\circ$) in longitude of perihelion. The current II -precession rate of Comet 2P/Encke is 7.8° in 1000 yr. A differential precession rate of at least this magnitude is required to explain the observed dispersion in only one rotation of the nodal line. Models suggest that several rotations are required, with the whole complex being at least 20–30,000 years old (Whipple, 1940; Steel and Asher, 1996).

The large $\sim 2 \times 10^{13}$ kg of dust in the complex (Jenniskens, 2006) hinted at a massive breakup of the original parent object that long ago, of which Comet Encke ($\sim 3 \times 10^{13}$ kg) was just one remnant. Numerous other asteroids in Taurid-like orbits were proposed to belong to this Encke Complex (Clube and Napier, 1984; Asher et al., 1993; Steel and Asher, 1996). These candidates had a wide range of semi-major axis ($a = 1.66\text{--}2.57$ AU), which was hard to explain (Steel and Asher, 1996). Indeed, a tally made in 2006 concluded that all proposed members up to that point were either S or O class asteroids, with reflectance properties unlike 2P/Encke (Jenniskens, 2006, pp. 462–464). Because of that, it is now thought that the originally proposed objects are instead asteroids that originated from the inner main belt by ejection via the v_6 resonance, a known source of S-class asteroids (Jenniskens, 2006).

Jenniskens (2006) proposed the hypothesis that the currently observed Taurid meteoroids are younger than the original disruption 20–30 kyr ago, but instead were created more recently from yet-to-be discovered parent bodies that are now still moving in very similar orbits as the stream. In this model, the Taurids are a family of sibling meteoroid streams, the dispersion of the whole

Table 12
Asteroids – established short semi-major axis showers with $T_j \gg 3$.

IAU	Object	N	λ_o	R.A.	Dec.	V_g	a	q	e	i	ω	Node	II	T_j
151	EAU	11	63	294.1	+20.4	31.5	0.82	0.405	0.513	64.6	322.8	62.5	26.3	6.67
326	EPG	33	109	330.2	+13.0	28.4	0.73	0.144	0.806	49.0	337.8	109.3	88.4	7.41
327	BEQ	38	91	305.1	+1.1	33.2	1.03	0.157	0.849	46.5	327.6	84.8	55.0	5.38
328	ALA ^a	2	106	349.4	+54.4	37.4	1.07	0.976	0.088	77.7	122.2	114.5	236.8	5.05

^a Uncertain that these two meteoroids originated from the same parent body.

Table 13

Shower dispersion – data on shower duration in solar longitude (λ_o , °), the drift corrected radiant and speed's measurement accuracy (\pm = standard error, in ° or km/s) and dispersion (σ = one standard deviation, in ° or km/s), the drift rate of the apparent radiant ($\Delta/\Delta\lambda_o$), and the shower-to-background surface density ratio (S/B) for new and confirmed shower components, where "E" means shower is established.

IAU #	λ_o Beg	λ_o Peak	λ_o End	$\Delta R.A. \pm$	$\Delta R.A. \sigma$	$\Delta Dec. \pm$	$\Delta Dec. \sigma$	$\Delta V_g \pm$	$\Delta V_g \sigma$	$\Delta R.A. / \Delta \lambda_o$	$\Delta Dec. / \Delta \lambda_o$	S/B
1	101	127	138	0.1	2.2	0.1	1.0	0.0	1.2	+0.97	+0.24	E
2	180	216	272	0.2	5.8	0.1	3.0	0.1	3.5	+0.99	+0.26	E
4	243	262	270	0.0	2.8	0.0	1.5	0.0	2.0	+1.15	-0.16	E
5	117	128	146	0.1	1.9	0.0	1.1	0.1	3.0	+0.95	+0.38	E
6	21	32	45	0.1	2.1	0.1	1.5	0.1	1.5	+0.66	+0.02	E
7	115	140	158	0.0	2.8	0.0	1.7	0.0	2.4	+1.40	+0.26	E
8	180	209	245	0.0	2.6	0.0	1.4	0.0	2.1	+1.03	-0.05	E
9	195	195	196	0.3	1.4	0.2	0.9	0.7	3.6	+0.34	-0.05	E
10	270	283	297	0.1	3.3	0.1	2.4	0.1	2.2	+0.56	-0.25	E
11	0	357	359	1.1	8.0	0.3	2.5	0.4	3.3	+0.92	-0.40	E
12	136	141	144	0.6	3.1	0.6	2.9	0.1	0.7	+0.40	+0.05	E
13	220	235	248	0.1	1.6	0.0	0.7	0.1	1.8	+0.99	-0.36	E
15	267	271	271	0.4	3.2	0.1	1.1	0.1	0.8	+0.05	-0.31	E
16	188	266	275	0.3	5.9	0.1	1.2	0.1	2.3	+0.92	-0.28	E
17	181	220	267	0.2	5.2	0.1	1.6	0.1	3.1	+1.03	+0.26	E
18	213	223	235	0.8	4.8	0.3	1.7	0.2	1.1	+1.00	+0.37	E
19	246	261	275	0.1	1.9	0.1	1.3	0.1	2.2	+0.97	-0.09	E
20	252	274	302	0.1	1.6	0.0	0.9	0.1	1.6	+0.96	-0.39	E
22	199	209	223	0.1	1.1	0.1	1.0	0.2	1.3	+1.02	-0.38	E
23	187	198	212	0.4	2.1	0.2	1.3	0.1	0.8	+1.13	-0.03	E
25	200	205	210	0.2	1.4	0.1	0.8	0.2	1.5	+1.00	+0.31	9
26	120	141	154	0.4	6.7	0.1	2.3	0.2	3.1	+0.91	+0.39	E
27	3	20	27	0.8	3.5	0.5	2.1	0.6	2.9	+0.81	-0.20	E
28	191	196	200	0.1	1.5	0.1	1.1	0.1	1.0	+0.95	+0.34	14
31	27	46	64	0.1	1.5	0.0	0.9	0.1	2.0	+0.92	+0.37	E
33	133	148	160	0.3	2.7	0.2	2.2	0.3	3.1	+0.92	+0.39	E
40	15	32	36	0.5	4.0	0.4	3.0	0.3	2.5	+0.64	+0.26	5
63	79	86	95	2.4	8.4	3.3	11.6	0.1	0.5	+0.92	-0.36	E
96	273	296	303	0.4	3.3	0.2	1.6	0.2	1.9	+1.04	-0.25	6
97	278	296	298	0.4	3.2	0.2	1.7	0.2	1.8	+1.00	-0.23	6
110	304	312	328	0.4	2.5	0.3	1.7	0.4	2.6	+0.89	-0.37	E
145	47	49	53	0.3	1.6	0.2	1.0	0.1	0.8	+0.56	+0.14	E
151	58	63	73	1.1	3.8	0.8	2.5	0.5	1.7	+0.78	+0.17	E
164	75	101	119	0.1	2.4	0.1	2.5	0.1	2.9	+0.95	+0.26	E
165	79	104	115	0.4	4.0	0.2	2.1	0.3	2.7	+1.05	+0.30	E
171	73	77	90	0.2	1.3	0.2	1.2	0.3	1.6	+1.05	+0.28	E
175	98	108	143	0.1	1.5	0.2	1.9	0.1	1.3	+0.90	+0.39	E
183	125	136	146	0.4	1.7	0.3	1.3	0.2	1.1	+0.94	+0.40	E
184	119	124	127	0.3	2.0	0.1	0.9	0.1	0.9	+0.45	+0.07	E
187	103	119	135	2.9	17.6	0.5	3.2	0.4	2.5	+1.68	+0.32	E
191	118	137	174	0.1	1.7	0.2	2.3	0.2	2.4	+0.86	+0.29	E
197	140	143	146	0.6	2.3	0.1	0.6	0.1	0.6	+0.26	+0.01	E
206	145	158	164	0.4	1.5	0.3	1.3	0.2	1.1	+1.24	-0.01	E
208	161	168	190	0.1	1.2	0.2	1.4	0.1	1.0	+1.17	+0.26	E
215	155	176	190	0.3	2.5	0.2	1.5	0.2	1.7	+0.93	+0.39	3
216	165	176	185	0.3	2.5	0.2	1.2	0.4	3.0	+0.92	+0.38	3
221	179	188	191	0.6	2.1	0.2	0.8	0.3	1.1	+0.91	-0.37	E
225	180	187	204	0.3	1.6	0.3	1.8	0.1	0.8	+0.92	+0.01	3
246	238	239	240	0.0	0.1	0.0	0.2	0.1	0.2	+0.97	-0.09	E ^a
250	225	247	265	0.1	2.6	0.1	1.4	0.1	2.5	+1.03	-0.01	E
252	266	272	274	0.3	0.4	0.1	0.2	0.9	1.5	+1.13	-0.31	E
253	243	252	265	0.7	3.8	0.3	1.7	0.6	3.6	+1.02	-0.09	4
256	253	258	261	0.3	1.9	0.2	1.1	0.7	4.0	+1.11	+0.04	5
257	238	243	268	0.2	1.6	0.1	1.2	0.1	1.4	+1.04	+0.11	E
286	238	242	245	0.2	1.5	0.2	1.4	0.1	1.0	+1.02	+0.16	15
319	279	283	287	0.4	1.4	0.1	0.5	0.3	0.9	+1.01	-0.34	E
320	277	176	281	0.1	0.1	0.7	1.0	0.2	0.2	+0.99	-0.37	E
323	293	296	300	0.4	2.2	0.3	1.3	0.3	1.4	+0.70	-0.13	E
324	86	88	91	0.4	0.9	0.2	0.4	0.3	0.7	+1.17	+0.23	E
326	101	109	120	1.2	7.0	1.0	5.6	0.5	2.7	+0.87	+0.35	E
327	77	91	98	0.5	2.9	0.4	2.4	0.3	2.1	+0.91	+0.23	E
328	108	106	121	1.6	2.3	0.2	0.2	0.2	0.3	+0.82	+0.39	E
330	272	276	275	0.6	1.0	0.6	1.0	0.1	0.2	+0.95	-0.16	E
331	265	284	297	0.2	2.2	0.2	2.1	0.2	2.3	+0.87	-0.24	E
333	201	202	203	0.5	1.6	0.2	0.7	0.4	1.3	+1.39	-0.33	E
334	248	256	263	0.7	5.1	0.4	2.7	0.2	1.5	+0.58	-0.34	E
335	248	267	280	0.3	2.1	0.2	1.0	0.3	2.0	+0.94	-0.39	E
336	250	252	255	0.4	2.7	0.2	1.3	0.2	1.0	+0.77	-0.39	E
337	150	163	234	0.2	3.1	0.2	4.2	0.1	2.4	+0.95	+0.19	E
338	216	232	242	0.3	2.4	0.3	2.9	0.2	2.0	+0.92	+0.20	E
339	250	253	258	0.3	1.2	0.3	1.1	0.2	0.7	+0.98	-0.39	E
341	295	298	302	0.4	2.2	0.2	1.0	0.4	2.3	+0.97	-0.39	E

(continued on next page)

Table 13 (continued)

IAU #	λ_o Beg	λ_o Peak	λ_o End	$\Delta R.A. \pm$	$\Delta R.A. \sigma$	$\Delta Dec. \pm$	$\Delta Dec. \sigma$	$\Delta V_g \pm$	$\Delta V_g \sigma$	$\Delta R.A. / \Delta \lambda_o$	$\Delta Dec. / \Delta \lambda_o$	S/B
346	348	350	352	0.4	0.9	0.2	0.5	0.5	1.2	+0.48	−0.10	E
348	36	38	44	0.5	3.2	0.3	2.1	0.3	1.7	+0.66	+0.32	E
372	78	103	130	0.1	2.5	0.1	2.4	0.1	1.6	+0.97	+0.38	E
388	207	221	235	0.3	2.1	0.2	1.5	0.4	2.6	+1.09	+0.18	E
390	229	244	249	0.5	4.1	0.3	2.5	0.4	3.7	+1.19	−0.04	E
392	239	242	268	1.0	8.3	0.4	3.5	0.3	2.2	+0.64	−0.38	3
404	289	298	300	1.1	5.6	0.4	1.9	0.2	1.2	+0.14	−0.26	E
411	94	107	124	0.2	2.4	0.1	1.8	0.1	1.4	+1.13	+0.35	E
427	314	315	316	0.3	0.8	0.2	0.6	0.3	0.9	+0.26	−0.20	E
444	102	109	118	0.2	2.2	0.1	1.5	0.1	1.4	+0.95	+0.40	15
445	221	225	228	0.2	0.4	0.3	0.9	0.3	0.8	+1.13	−0.34	E
446	246	252	258	0.4	3.2	0.2	1.5	0.1	1.1	+1.14	+0.37	E
470	145	149	158	1.2	8.6	0.4	3.0	0.2	1.3	+0.18	−0.09	10
479	180	187	195	0.2	1.4	0.2	1.4	0.2	1.1	+1.01	+0.06	22
505	144	151	173	0.2	1.9	0.2	1.3	0.3	2.1	+0.92	−0.40	8
506	300	314	328	0.2	1.8	0.2	1.3	0.2	1.4	+0.89	−0.37	6
552	140	159	179	0.3	2.9	0.2	2.2	0.2	2.2	+0.90	+0.13	3
558	225	227	229	0.3	0.8	0.4	0.9	0.3	0.8	+0.88	−0.21	6
623	112	120	128	0.1	1.2	0.1	0.9	0.1	0.7	+0.98	+0.22	28
624	200	205	209	0.1	1.7	0.1	1.0	0.1	1.5	+0.97	+0.31	124
625	225	231	236	0.1	1.1	0.1	0.8	0.1	0.8	+1.01	+0.21	50
626	211	216	218	0.1	1.6	0.1	1.4	0.1	1.7	+0.99	+0.26	359
627	180	189	190	0.2	1.9	0.1	1.3	0.1	1.0	+0.94	+0.36	54
628	218	223	225	0.1	1.3	0.1	1.1	0.1	1.4	+1.00	+0.23	47
629	232	233	236	0.1	1.1	0.1	1.0	0.1	1.1	+1.07	+0.19	246
630	218	220	222	0.1	1.0	0.1	1.1	0.1	1.1	+1.04	+0.25	51
631	213	216	217	0.1	1.0	0.1	0.9	0.2	1.3	+1.03	+0.26	25
632	223	227	230	0.1	1.3	0.1	0.9	0.1	1.1	+1.05	+0.22	194
633	238	240	241	0.2	1.1	0.2	1.1	0.1	1.0	+1.08	+0.15	132
634	241	244	246	0.2	1.3	0.2	1.3	0.2	1.3	+1.09	+0.13	12
635	227	231	237	0.2	1.7	0.1	1.1	0.2	2.1	+1.06	+0.20	8
636	248	252	254	0.2	1.2	0.2	0.9	0.2	1.2	+1.04	+0.06	7
637	225	225	229	0.2	1.7	0.1	0.9	0.1	1.0	+1.00	+0.23	19
638	255	260	265	0.2	1.8	0.2	1.5	0.2	1.3	+1.05	+0.02	5
640	132	137	154	0.1	2.4	0.1	1.7	0.1	2.3	+0.94	+0.39	18
641	259	262	266	0.2	1.2	0.1	0.5	0.3	2.3	+1.11	−0.17	^b
642	156	161	172	0.3	1.2	0.3	1.5	0.3	1.6	+0.91	+0.39	21
692	134	138	142	0.4	2.0	0.3	1.5	0.1	0.7	+0.95	+0.26	22
703	154	157	162	1.2	4.1	0.8	2.8	0.3	0.9	+0.50	−0.24	4
718	200	206	218	0.4	2.4	0.3	2.0	1.3	7.6	+1.01	−0.05	3
719	226	232	234	0.3	0.8	0.7	2.2	0.4	1.4	+1.04	−0.12	5
726	263	268	272	0.3	1.1	0.2	0.7	0.2	0.7	+1.11	−0.05	5
738	127	137	149	0.2	1.2	0.3	1.6	0.7	3.5	+0.90	+0.28	5

^a From photographic orbits during meteor outbursts (Jenniskens et al., 1997).

^b High velocity component of the Geminids.

complex reflecting the evolution of the parent bodies after the initial fragmentation event. The first such potential parent body was proposed: 2004 TG₁₀ (Jenniskens, 2006, 2008).

In the context of weakly cohesive rubble pile asteroids and comets held together by small grains (Scheeres, 2014), “disruption” here is perhaps a better description than the term “fragmentation”. Disruptions provide a natural mechanism for having a significant part of the original mass decay in the form of dust, while leaving some larger parts that are more cohesive.

Since that time, Porubcan et al. (2006) and Babadzhanov et al. (2008) have divided the photographed Taurids into 19 clusters, based mostly on groupings of only 2–6 fireball orbits each. They identified a number of candidate parent bodies, again having a relatively wide range in semi-major axis ($a = 1.3$ – 2.6 AU). Of the 11 Encke Complex “filaments” identified in our solar longitude interval by the most recent compilation of Bucek and Porubcan (2014) from independent photographic, video and radar data, as many as 8 are close to one of our 19 components. Their “mu Piscids (b)” are much like our NPS, their “S Psc” are XAR, “S Tau” are STS, “N Tau” are ATU, “o Ori S” are ORS, “o Ori N” are ORN, “eta Gem N” are DZT, and “mu Gem” are DEG. This gives confidence that at least some of our components persist from year to year and originated from separate parent bodies.

For each of the 19 components listed in Table 2, we searched for potential parent body asteroids that still move in similar orbits. If we assume that the relative error in semi-major axis and perihelion distance should be less than 20% and the absolute error in Π should be less than 4° , i.e. the typical dispersion of orbital elements in Taurid-like orbits, with initial $\Delta a = 0.0002$ AU over a period of 20,000 y (Steel and Asher, 1996; Asher et al., 1993), then only the 7 objects listed in Table 2 marked “*” fit the bill. This excludes many of the previously proposed tentative associations by Jenniskens (2006), Porubcan et al. (2006), and Babadzhanov et al. (2008).

These 7 objects are a very different population than proposed earlier. The new candidates all have a Tisserand parameter with respect to Jupiter (T_J) in the range $T_J = 2.96$ – 3.12 , on the border of the comet–asteroid domains. All have a semi-major axis in the narrow range $a = 2.20$ – 2.35 AU (Table 2), and most are relatively small 0.3–1 km in size. Aside from 3.0-km large Comet 2P/Encke, these objects have a combined volume (or mass if the density is the same) of 20% of that of Comet Encke. The smallest object is 340-m wide 2003 WP₂₁ (Table 2).

Of the 17 known asteroids with semi-major axis between $a = 2.20$ and 2.35 AU and Π between 130° and 185° , 53% (7) can be associated with one of the Taurid stream components (Table 2).

and two more with the related χ -Orionid showers (Table 3). We anticipate that more parent asteroids will be discovered in the future, because only $\sim 64\%$ of near-Earth asteroids 0.3–1 km have so far been discovered.

Only one of the 19 individual components appears to be the result of meteoroids being trapped in mean-motion resonances. Periodically, the Taurids have 5° -wide outbursts centered on solar longitude $\lambda_o = 222^\circ$ (Dubietis and Arlt, 2007). These are understood to be due to dust trapped in the 7:2 mean-motion resonance with Jupiter at $a = 2.257$ AU (Asher and Izumi, 1998). The resonance prevents the spreading of the dust over mean anomaly, with the resonance center of the swarm of meteoroids moving 360° in 3.391 yr. The SonotaCo network (Kanamori, 2009) observed such a Taurid outburst in 2008 during solar longitude 219 – 226° , with a strong concentration of radiants in the Southern Taurid component. From this data, average orbital elements are presented in Table 2. One of the CAMS identified Southern Taurid components, now called the s-Taurids (#628, STS), might be a weak manifestation of this resonant dust filament in the 2012 CAMS data (Table 2). The next meteor outbursts are expected to occur in 2015 and 2022.

The orbital elements for this component are most similar to those expected from active Comet 2P/Encke itself, suggesting this is the source of the outburst meteors, the nodal line having evolved sufficiently to intersect Earth's orbit at the ascending node (Southern Taurids), but not yet at the descending node (Northern Taurids). In general, features in the Southern Taurids do not mirror those in the Northern Taurids, implying that the streams fade before the nodal line has rotated sufficiently. This disappearing of the larger meteoroids is not due to dispersion by gravity, but implies a disruption of the meteoroids into smaller grains by forces other than collisions with other meteoroids on the $1/e$ timescale of ~ 4000 years.

5.3. Origin of the Phaethon Complex

The Geminid shower (#4, GEM) derives from Asteroid 3200 Phaethon (Whipple, 1983). The shower has a Tisserand parameter with respect to Jupiter of about $T_J \sim 4.4$, squarely in the asteroid domain. It was recently proposed that this object originated from the 33° -inclined Pallas asteroid family, being debris from Asteroid 2 Pallas (Licandro et al., 2010). There is reasonable agreement between the reflectance spectrum of 3200 Phaethon and that of 2 Pallas, as was recently independently pointed out by DeLeón et al. (2010) and Jenniskens et al. (2010b). The proposed pathway for bringing Phaethon into the inner Solar System by Licandro et al. (2010), however, implied a several million-year long dynamical evolution.

A faster pathway via the 5:2 resonance is more likely, given the ongoing disruption of this body. Phaethon spawned the Geminids only about 1000 years ago (Jenniskens, 2006). And Phaethon is not alone. Also relatively recently, the Daytime Sextantid shower (#221, DSX) were spawned by Asteroid 2005 UD (Ohtsuka, 2005; Ohtsuka et al., 2006), which has the same spectral reflectance spectrum as Phaethon (Jewitt and Hsieh, 2006; Kinoshita et al., 2007). CAMS detected 14 DSX in the hour before dawn (Table 5).

Both 2005 UD and Phaethon have a node relatively close to that of their associated meteoroid streams. 2005 UD moves in an orbit similar to Phaethon, but with the position of the nodal line lagging that of Phaethon by ~ 4600 -years (Table 4), a sizeable differential lag in the $\sim 20,000$ -year rotation of the nodal line. 2005 UD lags the Daytime Sextantids by only 700 years. In comparison, Phaethon lags the Geminids by 220 years (Jenniskens, 2006). In both cases, parent body and shower are significantly more similar to their meteoroid stream than to each other in their position in the cycle.

This suggests a relatively quick fading of the meteoroid stream over time, on a timescale capable of causing a difference in the rotation of the nodal line of order 1000 years, which takes about 4500 years judging from the present 220-year lag of the Geminids since formation 1000 years ago (Jenniskens, 2006). Hence, ~ 0.1 g meteoroids of 3200 Phaethon (+3 magnitude Geminids) last only ~ 4500 years in interplanetary space before falling apart.

Much of the dust that originated from the original disruption that created the progenitors of Phaethon and 2005 UD has now faded. The nature of the December Canis Minorids is unclear. It could be a tail of dust that has spread from the progenitor of 2005 UD, dust from a yet-to-be discovered parent body from that same generation, or perhaps even be a remnant of dust from the original disruption.

The presence of the faster-than-expected Geminids (DRG) with $V_g \sim 39$ km/s in the main shower is interesting. There are also much slower than typical Geminids ($V_g \sim 31$ km/s) that are not isolated here. They are detected around the peak of the Geminid shower. Initially, we suspected perturbations by Earth as a dynamical mechanism to create an outlier group. However, 56 out of 60 DRG have an unusual deceleration with a high product of $a_1 a_2 > 2$ km/s. If this is not simply the result of measurement error, then perhaps these meteoroids represent material with unusual physical properties. These faster Geminids could have had lower density, resulting in higher deceleration in the Earth's atmosphere and a somewhat different orbital evolution from higher radiation pressure in space.

5.4. Origin of the Machholz Complex showers

Comet 96P/Machholz is in a highly inclined orbit (Table 5), which oscillates between states of high i , high q and low i , low q when the nodal line rotates, twice in one full nutation cycle, which takes about 8000 years (Wu and Williams, 1992). Along this path are found Asteroid 2003 EH₁ and two families of small 10-m sized low- q ("sunskirter") comets called the Marsden and Kracht groups, which are fragments of earlier larger comets that disrupted into such small fragments that they are detected now mainly when they pass close to the Sun by sun-pointed satellites.

These objects are found at different positions along the cycle, the differential evolution presumably caused by differences in the rate of nodal line rotation (Jenniskens, 2006). There is a rapid and uniform decrease of Π with position in the cycle, from $\Pi = 109^\circ$ of 96P/Machholz to $\Pi = 95^\circ$ of 2003 EH₁ (Table 5). The meteoroid streams fit into this sequence as follows in terms of the temporal location along the cycle, with 1 being a complete cycle: 0.00 (96P), 0.10 (ARI, Marsden group), 0.13 (Kracht group), 0.20 (SDA, C/2008 Y₁₂), 0.40 (QUA, 2003 EH₁), 0.72 (NDA) and 1.18 (AIC).

Sekanina and Chodas (2005) proposed that 96P/Machholz broke only a few hundred years prior to 1059 A.D., and that the rapid differential evolution was caused by a specific close encounter of the train of fragments with Jupiter in 1059 A.D., accelerating the secular evolution more so for fragments that passed nearest to the planet. At a later time, some of these fragments broke further to create the Marsden and Kracht sunskirters.

This hypothesis can be tested from the age of associated meteoroid streams, but it first needs to be understood how these streams are related to the potential parent bodies. The ARI, SDA, and QUA have parent bodies at nearly the same position along the nutation cycle (Table 5), despite the fact that one of the nodes of the stream has to be near Earth's orbit for the stream to be detected. This lack of differential evolution suggests that these streams are young and originated from recent disruptions leaving the observed parent bodies as they are found now. Indeed, it is

thought that the Quadrantids were created from 2003 EH₁ only 200–600 years ago (Jenniskens, 2004; Wiegert and Brown, 2005).

Until now, radar observations of Daytime Arietids measured too short a semi-major axis to suggest the meteoroids were derived from the Marsden group formation event (Campbell-Brown, 2004). Instead, the CAMS measured value for the semi-major axis of the detected meteoroids is not significantly different from the value of $a = 3.04$ AU of Marsden sunskirter Comet P/1999 J₆ (Fig. 12). This, at last, confirms that the stream can in principle be debris from the breakup that gave rise to the sunskirter comets (Jenniskens et al., 2012b). Formation models, however, need to explain the wide activity profile (Jenniskens, 2006) and the change in measured orbital elements with solar longitude (Fig. 12). They are not a product of particle-size dependent ejection conditions. There is no trend of Δq with meteor brightness.

Comet C/2008 Y₁₂ moves in an orbit similar to that of the SDA and may be responsible for the main activity of this stream (Fig. 14). In analogy with the Marsden and Kracht groups, this object may be part of a yet-to-be discovered comet family. Again, the wide profile of the stream needs to be explained.

Other showers may be caused by family forming events that occurred at different parts of the nutation cycle. Based on their longitude of perihelion (and the fact that their dispersion in Π is higher), the late Southern delta Aquariids called the August o-Aquariids (AOA) may in fact have originated from the Kracht sunskirter group breakup ($\Pi = 102.3^\circ$), and/or that of the Marsden group at $\Pi = 103.6^\circ$.

The Quadrantids contain a background component to the activity profile (Jenniskens, 1994), the width of which was thought to require a higher formation age of about 3500 years (Wiegert and Brown, 2005). Like the AOA, this background component may represent dust from other disruption events in the Machholz family.

Further along the nutation cycle, the Northern Delta Aquariids may have been released during the earlier creation of the Machholz Complex. It is unclear how this dust can evolve over 0.72 of a nutation cycle in the ~ 1500 y proposed by Sekanina and Chodas (2005). This needs further study.

There is no evidence that the meteoroid streams last much more than one cycle, which implies a fast differential evolution and short lifespan of the meteoroids. If the orbital evolution would have persisted for multiple nutation cycles, then Babadzhanyan and Obruchov (1992) predicted there should also be an “ α -Cetids” stream (R.A. = 39–53°, Dec. = +8–13°, $V_g = 39$ –44 km/s in the interval $\lambda_o = 249$ –263°), which is not detected in CAMS data. They also predicted a shower near the position of the Ursids (#15, URS) in late December, but that shower (from 4.5-km sized Comet 8P/Tuttle) has a longer, $a = 5.70$ AU, semi-major axis than other Machholz showers. An alternative nearby candidate shower is not observed.

The Machholz Complex showers are located on the toroidal ring (Fig. 1). Most other showers in that ring appear to be of Halley-type (Pokorný et al., 2013). Perhaps Comet 96P/Machholz was a Halley-type comet in the past, possibly prior to splitting from 8P/Tuttle, which now has $\Pi = 117.8^\circ$.

5.5. Why some showers are not detected

The Southern ι-Aquariids are the only established shower that CAMS did not clearly see, but should have, because the stream was previously reported from photographic observations of meteoroids of similar brightness by several authors (Jenniskens, 2006). All other established showers that are not detected are either rich in faint meteors, daytime showers, southern hemisphere showers, or periodic showers that did not show up in the period of observations. We therefore recommend that the Southern ι-Aquariids be

moved back from the IAU List of Established Showers to the Working List for more study.

Some showers are very strong in the CMOR radar data, but (nearly) absent in CAMS data. One example is the Bootids–Coronae Borealis Complex on the northern toroidal ring (Brown et al., 2010). The ξ-Coronae Borealis (#323, XCB) are detected, but the related λ Bootids (#322, LBO) are very weak in CAMS data. There is only a hint of LBO in the Π - i diagram of a narrow 5° interval of solar longitude. The θ-Coronae Borealis (#321, TCB) are not detected at all. These showers must have a steep magnitude distribution index ($\chi \gg 3$), lacking sufficient numbers of bright meteors. The steep magnitude distribution index implies that the larger grains are efficiently lost by other processes than collisions (Jenniskens, 2006). Their short semi-major axis suggests that these are relatively old showers, influenced strongly by Poynting–Robertson drag (Sekanina, 1976).

Other such showers include CMOR’s α-Ursae Majorids (#385, AUM) with $a = 1.10$ AU, $e = 0.21$, and the October κ-Draconids (#387, OKD) with $a = 1.26$ AU and $e = 0.27$. Note that shower #383 is the same as shower #242 and should be removed from the Working list. The ξ-Draconids (#242, XDR), with $a = 2.05$ AU and moderate eccentricity $e = 0.55$, may also be rich in faint meteors.

Periodic showers that were not detected include the τ-Herculids (#61, TAH), the October Capricornids (#233, OCT), the α-Monocerotids (#246, AMO), the October Camelopardalids (#281, OCT), and the June Bootids (#170, JBO). A diffuse scatter of radiants was picked up from the sporadic background by the D_p criterion starting from a typical JBO orbit, but there is no associated increase in surface density, suggesting that those may not be related to Comet 7P/Pons–Winnecke. Some meteors were detected near the radiant position of the Phoenicids (#254, PHO) from Comet D/1819 W₁ (Blanpain), but no clear shower is defined in the density distribution of meteoroid radiants and orbits. At the position of the historic Corvids (#63, COR), however, there is a weak concentration of meteoroids in the Π - i diagram (Table 7), which is perhaps from the same source.

6. Conclusions

In the first 2.5 years of observations, CAMS detected 70 of the 95 established showers. Median orbital elements and dispersions are presented for each stream. Besides daytime showers, southern hemisphere showers, periodic showers and showers rich in faint meteors, only the Southern iota Aquariids were not conclusively detected.

Several shower complexes are observed that previously were thought to be due to parent body disruption cascades, whereby a disruption leaves as much mass in the form of dust as in the largest remaining fragment, the “parent body” (Jenniskens, 2006, 2008).

The Encke Complex was decomposed into 19 individual Taurid shower components, based on variations in relative activity from Northern and Southern Taurids on a given day, variations in compactness of the radiant, and apparent jumps in position of the drift-corrected radiant. 7 of these components were associated with parent body asteroids that are still in very similar orbits. Unlike proposed parent bodies in the past, these asteroids all have a narrow range of semi-major axis similar to 2P/Encke ($a = 2.20$ – 2.35 AU). Of 17 known asteroids with semi-major axis in this range and $\Pi = 130$ – 185° , nine (53%) can be associated with one of the Taurid or χ-Orionid stream components. The current completeness of Near Earth Object detections in the relevant 0.3–1 km range is about 64%, in good agreement. Meteoroids falling apart before the nodal line can fully rotate can explain why streams and parent bodies are still found intimately

associated and why the Northern and Southern showers do not have corresponding activity at the same solar longitude.

The Machholz Complex gained two additional shower components: the August α -Aquadriids and the August ι -Cetids. The Daytime Arietids, Southern δ -Aquadriids and Quadrantids have associated parent bodies that are still in close proximity to their streams. The August α -Aquadriids and a background to activity of the Quadrantids may be debris from the formation of the Kracht or Marsden groups of sunskirters, instead, that are now found further along the cycle. The Northern δ -Aquadriids and August ι -Cetids are found at a more evolved position along the nutation cycle. It is unclear, at present, whether or not these streams represent dust from the original breakup that left 96P/Machholz. All detected streams point to the dust surviving for only enough time to show a differential evolution of ~ 1 nutation cycle. CAMS did not detect two other candidate showers, expected if the meteoroids survive in streams much longer.

The Phaethon Complex behaves in much the same way, despite a possible origin with the Pallas asteroid family. Even though Geminids are known to have a relatively high meteoroid density and move in $T_J \sim 4.4$ orbits, the Phaethon parent body has decayed in streams and remaining comet fragments much like Jupiter-family comets do. The Geminids and Daytime Sextantids associated parent bodies are all still in close proximity to the streams (in terms of the direction of their nodal line), pointing to relatively recent disruptions that left these bodies as the largest remaining fragments. There is also an older component, a possible twin shower of the Geminids, called the December Canis Minorids. Even the separation of the progenitor Phaethon and 2005 UD happened relatively recently compared to the million-year timescale of the proposed asteroid orbital evolution into the inner Solar System. If these objects originated from the Pallas asteroid family, then there must be a more rapid pathway from family to the orbit of 3200 Phaethon than proposed.

In addition to these known shower complexes, two new components to the α -Capricornids were identified, making this a 169P/NEAT Complex. While 169P/NEAT is likely directly associated with the α -Capricornids itself, the earlier ξ^2 -Capricornids appear to be associated with Comet 2003 T₁₂ (SOHO). There is also a third dust component, the late ε -Aquadriids.

Most CAMS-detected meteors represent large mm–cm sized meteoroids that were relatively recently released by their parent bodies. Meteor outbursts from the crossing of dust trails and filaments are frequently detected in the CAMS data, especially among JFC-type showers. The predicted 2011 Draconid outburst produced orbital elements consistent with the calculated 1900-dust ejecta of parent Comet 21P/Giacobini–Zinner. A strong unexpected outburst of slow December ϕ -Cassiopeiids was observed in December of 2011, perhaps from past activity of 3D/Biela. During March 12–19, 2013, an outburst of 56 η -Virginids (#11, EVI) was detected from an unknown source.

Furthermore, the 1-revolution dust trail of a Long Period comet caused an outburst of February η -Draconids over a period of a few hours on February 4, 2011, while the long-period October Ursae Majorids (#333, OCU) and the low- q January Leonids (#319, JLE) appear to have had an outburst in 2012.

Orbits from the predicted outburst of Comet Halley's Orionids on October 21, 2010, were not precisely enough measured to prove that the outburst was caused by meteoroids trapped in the 6:1 mean motion resonance, as has been proposed.

Several other detected showers in the apex source may have an origin with 1P/Halley, forming an "Orionid tail" in the drift-corrected radiant distribution. Similarly, at least one shower, the ζ -Cassiopeiids, forms a complex with the Perseids of Halley-type Comet 109P/Swift–Tuttle.

The origin of the toroidal showers is the most problematic. Several toroidal showers seem to have components with both HTC-type and JFC-type orbital periods. Many toroidal showers are rich in small meteoroids and have unusually short semi-major axis, some with orbital periods more typical of asteroids.

Future improvement of our understanding of meteoroid streams at Earth will come from ongoing CAMS operations and its expansion to the southern hemisphere. Theoretical modeling is needed to establish the proposed links with parent body Near Earth Objects discussed in this paper, and to interpret the showers as a record of past parent body evolution.

Acknowledgments

We thank all CAMS team members for their support of the project: amateur astronomers and students who helped build CAMS, supported CAMS operations over the years and assisted in the ongoing data reduction effort. In particular, we thank Beth Johnson, Kathryn Steakley, and Meridel Phillips of the SETI REU program, who supported the data reduction effort. Michael Borden and Kevin Newman of the NASA Ames Exploration Academy helped develop the CAMS hardware. Fremont Peak State Park and Lick Observatory generously hosted the deployment of the CAMS camera stations. The CAMS project was made possible by grants from NASA's Planetary Astronomy (NNX08AO64G) and Near Earth Object Observation (NNX12AM14G) programs.

References

- Andreic, Z. et al., 2013. August ι Cetids, a possible new meteor shower in August. *J. Int. Meteor. Org.* 41, 40–42.
- Andreic, Z. et al., 2014. Results of CMN 2013 search for new showers across CMN and SonotaCo databases I. *J. Int. Meteor. Org.* 42, 90–97.
- Asher, D.J., Izumi, K., 1998. Meteor observations in Japan: New implications for a Taurid meteoroid swarm. *Mon. Not. R. Astron. Soc.* 297, 23–27.
- Asher, D.J., Clube, S.V.M., Steel, D.I., 1993. Asteroids in the Taurid Complex. *Mon. Not. R. Astron. Soc.* 264, 93–105.
- Babadzhanov, P.B., Obrubov, Yu.V., 1992. P/Machholz 1986 VIII and Quadrantid meteoroid stream. Orbital evolution and relationship. In: *Asteroids, Comets, Meteors 1991*. Lunar and Planetary Institute, Houston, pp. 27–32.
- Babadzhanov, P.B., Williams, I.P., Kokhirova, G.I., 2008. Near-Earth Objects in the Taurid Complex. *Mon. Not. R. Astron. Soc.* 386, 1436–1442.
- Brown, P. et al., 2008a. A meteoroid stream survey using the Canadian Meteor Orbit Radar – I: Methodology and radiant catalogue. *Icarus* 195, 317–339.
- Brown, P. et al., 2008b. The Canadian Meteor Orbit Radar meteor stream catalogue. *Earth Moon Planets* 102, 209–219.
- Brown, P. et al., 2010. A meteoroid stream survey using the Canadian Meteor Orbit Radar – II: Identification of minor showers using a 3D wavelet transform. *Icarus* 207, 66–81.
- Bucek, M., Porubcan, V., 2014. Taurid meteor complex. In: Jopek, T.J. et al. (Eds.), *Meteoroids 2013*. Proceedings of the Astronomical Conference held at A.M. University, Poznan, Poland, August 26–30, 2013. A.M. University Press, pp. 193–197.
- Campbell-Brown, M.D., 2004. Radar observations of the Arietids. *Mon. Not. R. Astron. Soc.* 352, 1421–1425.
- Ceplecha, Z., 1987. Geometric, dynamic, orbital and photometric data on meteoroids from photographic fireball networks. *Bull. Astron. Inst. Czechoslovakia* 38, 222–234.
- Clifton, K.S., 1973. Television studies of faint meteors. *J. Geophys. Res.* 78, 6511–6521.
- Clube, S.V.M., Napier, W.M., 1984. The microstructure of terrestrial catastrophism. *Mon. Not. R. Astron. Soc.* 211, 953–968.
- DeLeón, J. et al., 2010. Origin of the near-Earth asteroid Phaethon and the Geminids meteor shower. *Astron. Astrophys.* 513, id. A26.
- Dubietis, A., Arlt, R., 2007. Taurid resonant-swarm encounters from two decades of visual observations. *Mon. Not. R. Astron. Soc.* 376, 890–894.
- Gajdos, S. et al., 2014. The September Σ -Perseids in 2013. *J. Int. Meteor. Org.* 42, 48–56.
- Galligan, D., 2003. Radar meteoroid orbit stream searches using cluster analysis. *Mon. Not. R. Astron. Soc.* 340, 899–907.
- Gural, P.S., 1995. Applying state-of-the-art video and computer technology to meteor astronomy. *J. Int. Meteor. Org.* 23, 228–235.
- Gural, P.S., 1997. An operational autonomous meteor detector: Development issues and early results. *J. Int. Meteor. Org.* 25, 136–140.
- Gural, P.S., 2012. A new method of meteor trajectory determination applied to multiple unsynchronized video cameras. *Meteorit. Planet. Sci.* 47, 1405–1418.
- Gural, P.S. et al., 2014. Results of the CMN 2013 search for new showers across CMN and SonotaCo databases II. *J. Int. Meteor. Org.* 42, 132–138.

- Hajduková, M.R., Kornos, L., Tóth, J., 2014. Hyperbolic orbits in the EDMOND. In: Jopek, T.J. et al. (Eds.), *Meteoroids 2013. Proceedings of the Astronomical Conference held at A.M. University, Poznan, Poland, August 26–30, 2013*. A.M. University Press, pp. 289–295.
- Hawkes, R.L., Jones, J., 1975. Television observations of faint meteors. I. – Mass distribution and diurnal rate variation. *Mon. Not. R. Astron. Soc.* 170, 363–377.
- Holman, D., Jenniskens, P., 2012a. Confirmation of the Northern Delta Aquariids (NDA, IAU #26) and the Northern June Aquilids (NZC, IAU #164). *J. Int. Meteor. Org.* 40, 166–170.
- Holman, D., Jenniskens, P., 2012b. Confirmation of the July Gamma Draconids (GDR, IAU #184). *J. Int. Meteor. Org.* 40, 36–41.
- Holman, D., Jenniskens, P., 2013. Discovery of the Upsilon Andromedids (UAN, IAU #507). *J. Int. Meteor. Org.* 41, 43–47.
- Jacchia, L.G., Verniani, F., Briggs, R.E., 1961. An analysis of the atmospheric trajectories of 413 precisely reduced photographic meteors. *Smiths. Contrib. Astrophys.* 10, 1–45.
- Jenniskens, P., 1994. Meteor stream activity. I. The annual streams. *Astron. Astrophys.* 287, 990–1013.
- Jenniskens, P., 2004. 2003 EH₁ is the parent of the Quadrantids. *Astron. J.* 127, 3018–3022.
- Jenniskens, P., 2006. *Meteor Showers and their Parent Comets*. Cambridge University Press, Cambridge, UK, 790pp.
- Jenniskens, P., 2008. Mostly dormant comets and their disintegration into meteoroid streams (a review). *Earth Moon Planets* 102, 505–520.
- Jenniskens, P., 2012. Mapping meteoroid orbits. *Sky Telesc.* 87, 20–25.
- Jenniskens, P., Gural, P.S., 2011. Discovery of the February η -Draconids (FED, IAU#427): The dust trail of a potentially hazardous long-period comet. *J. Int. Meteor. Org.* 39, 93–97.
- Jenniskens, P., Haberman, B., 2013. “Thatcher’s Ghost”: Confirmation of the ν -Cygnids (NCY, IAU #409). *J. Int. Meteor. Org.* 41, 75–76.
- Jenniskens, P., Vaubaillon, J., 2007. 3D/Biela and the Andromedids: Fragmenting versus sublimating comets. *Astron. J.* 134, 1037–1045.
- Jenniskens, P., Vaubaillon, J., 2008. Minor planet 2008 ED69 and the Kappa Cygnid meteor shower. *Astron. J.* 136, 725–730.
- Jenniskens, P., Vaubaillon, J., 2010. Minor planet 2002 EX12 (=169P/NEAT) and the Alpha Capricornid shower. *Astron. J.* 139, 1822–1830.
- Jenniskens, P. et al., 1997. The detection of a dust trail in the orbit of an Earth-threatening long-period comet. *Astrophys. J.* 479, 441–447.
- Jenniskens, P. et al., 2009. On how to report new meteor showers. *J. Int. Meteor. Org.* 37, 19–20.
- Jenniskens, P. et al., 2010a. Almahata Sitta (=Asteroid 2008 TC3) and the search for the ureilite parent body. *Meteorit. Planet. Sci.* 45, 1590–1617.
- Jenniskens, P., Sato, M., Watanabe, J.-I., 2010b. Orionid meteors 2010. In: Green, D. W.G. (Ed.), *CBET 2507, Central Bureau Electronic Telegrams*, 1pp.
- Jenniskens, P. et al., 2011a. CAMS: Cameras for Allsky Meteor Surveillance to establish minor meteor showers. *Icarus* 216, 40–61.
- Jenniskens, P. et al., 2011b. In: Green, D.W.E. (Ed.), *CBET 2862, Central Bureau Electronic Telegrams*, 1pp.
- Jenniskens, P., Gural, P.S., Holman, D., 2012a. The established meteor showers as seen in video meteoroid orbit surveys. In: Gyssens, M., Roggemans, P. (Eds.), *Proceedings of the International Meteor Conference, La Palma, 20–23 September 2012*. The International Meteor Organization, Belgium, pp. 38–43.
- Jenniskens, P., Duckworth, H., Grigsby, B., 2012b. Daytime Arietids and Marsden sunskirters (ARI, IAU #171). *J. Int. Meteor. Org.* 40, 98–100.
- Jewitt, D., Hsieh, H., 2006. Physical observations of 2005 UD: A mini-Phaethon. *Astron. J.* 132, 1624–1629.
- Jobse, K., de Lignie, M.C., 1987. Een TV systeem voor meteoren. *Radiant. J. Dutch Meteor. Soc.* 9, 38–41.
- Jones, D.C., Williams, I.P., Porubcan, V., 2006. The κ -Cygnid meteoroid complex. *Mon. Not. R. Astron. Soc.* 371, 684–694.
- Jopek, T.J., Kanuchová, Z., 2014. Current status of the IAU MDC Meteor Shower Database. In: Jopek, T.J. et al. (Eds.), *Meteoroids 2013. Proceedings of the Astronomical Conference held at A.M. University, Poznan, Poland, August 26–30, 2013*. A.M. University Press, pp. 353–364.
- Jopek, T.J., Rudawska, R., Pretka-Ziomek, H., 2006. Calculation of the mean orbit of a meteoroid stream. *Mon. Not. R. Astron. Soc.* 371, 1367–1372 (Erratum: 2008 *Mon. Not. R. Astron. Soc.* 387, 1741).
- Jopek, T.J., Rudawska, R., Bartczak, P., 2008. Meteoroid stream searching: The use of the vectorial elements. *Earth Moon Planets* 102, 73–78.
- Kanamori, T., 2009. A meteor shower catalog based on video observations in 2007–2008. *J. Int. Meteor. Org.* 37, 55–62.
- Kinoshita, D. et al., 2007. Surface heterogeneity of 2005 UD from photometric observations. *Astron. Astrophys.* 466, 1153–1158.
- Kornos, L. et al., 2012. Database of meteoroid orbits from several European video networks. In: Gyssens, M., Roggemans, P. (Eds.), *Proceedings of the International Meteor Conference, La Palma, 20–23 September 2012*. The International Meteor Organization, Belgium, pp. 21–25.
- Kornos, L. et al., 2014. Confirmation and characterization of IAU temporary meteor showers in EDMOND database. In: Jopek, T.J. et al. (Eds.), *Meteoroids 2013. Proceedings of the Astronomical Conference held at A.M. University, Poznan, Poland, August 26–30, 2013*. A.M. University Press, pp. 225–233.
- Koschny, D. et al., 2004. Radianths of the Leonids 1999 and 2001 obtained by LLLTV systems using automatic software tools. *Earth Moon Planets* 95, 255–263.
- Koten, P. et al., 2003. Catalogue of video meteor orbits. Part 1. *Publ. Astron. Inst. ASCR* 91, 1–32.
- Licandro, J. et al., 2010. The nature of comet–asteroid transition object (3200) Phaethon. *Astron. Astrophys.* 461, 751–757.
- Lyytinen, E., Jenniskens, P., 2003. Meteor outbursts from Long Period comet dust trails. *Icarus* 162, 443–452.
- Marsden, B.G., Sekanina, Z., 1971. Comets and nongravitational forces IV. *Astron. J.* 76, 1135–1151.
- Molau, S., 1993. MOVIE: Meteor observation with video equipment. In: *Proc. International Meteor Conference*. International Meteor Organization, Potsdam, pp. 71–75.
- Molau, S., Barentsen, G., 2014. Status and history of the IMO Video Meteor Network. In: Jopek, T.J. et al. (Eds.), *Meteoroids 2013. Proceedings of the Astronomical Conference held at A.M. University, Poznan, Poland, August 26–30, 2013*. A.M. University Press, pp. 297–305.
- Neslusan, L., Svoren, J., Porubcan, V., 1998. A computer program for calculation of a theoretical meteor-stream radiant. *Astron. Astrophys.* 331, 411–413.
- Ohtsuka, K., 2005. 2005 UD and the Daytime Sextantids. *CBET 283, Minor Planet Center*, Cambridge, MA, p. 1–1.
- Ohtsuka, K. et al., 2006. Apollo Asteroid 2005 UD: Split nucleus of (3200) Phaethon? *Astron. Astrophys.* 450, L25–L28.
- Pokorny, P. et al., 2013. Dynamical model for the toroidal source of the sporadic meteoroid complex. *AAS DPS Meeting. Abstract #45, #402.04*.
- Porubcan, V., Kornos, L., Williams, I.P., 2006. The Taurid Complex meteor showers and asteroids. *Contr. Obs. Skalnaté Pleso* 36, 103–117.
- Rozek, A., Breiter, S., Jopek, T.J., 2011. Orbital similarity functions – Application to asteroid pairs. *Mon. Not. R. Astron. Soc.* 412, 987–994.
- Rudawska, R., Vaubaillon, J., Jenniskens, P., 2013. Asteroid 2010 TU149 in the Taurid Complex. In: *European Planetary Science Congress 2012, 23–28 September 2012, Madrid, Spain. Abstract Id. EPSC 2012-886*.
- Sato, M., Watanabe, J.-I., 2007. Origin of the 2006 Orionid outburst. *Publ. Astron. Soc. Jpn.* 59, L21–L24.
- Scheeres, D.J., 2014. Solar System: Sandcastles in space. *Nature* 512, 139–140.
- Segon, D. et al., 2012. New shower in Cassiopeia. *J. Int. Meteor. Org.* 40, 195–200.
- Sekanina, Z., 1976. Statistical model of meteor streams. IV – A study of radio streams from the synoptic year. *Icarus* 27, 265–321.
- Sekanina, Z., Chodas, P.W., 2005. Origin of the Marsden and Kracht groups of sunskirting comets. I. Association with Comet 96P/Machholz and its interplanetary complex. *Astrophys. J. Supp. Ser.* 161, 551–586.
- Sekhar, A., Asher, D.J., 2014. Resonant behavior of Comet Halley and the Orionid stream. *Meteorit. Planet. Sci.* 49, 52–62.
- Sosa, A., Fernández, J.A., 2015. Comets 169P/NEAT and P/2003 T12 (SOHO): Two possible fragments of a common ancestor? *IAU General Assembly, August 3–14, 2015, American Astronomical Society, Honolulu Hawaii. Abstract #2255583*.
- Southworth, R.B., Hawkins, G.S., 1963. Statistics of meteor streams. *Smiths. Contrib. Astrophys.* 7, 261–285.
- Steakley, K., Jenniskens, P., 2013. Discovery of the February ε Virginids (FEV, IAU#506). *J. Int. Meteor. Org.* 41, 109–111.
- Steel, D., Asher, D., 1996. The orbital dispersion of the macroscopic Taurid objects. *Mon. Not. R. Astron. Soc.* 280, 806–822.
- Teren’teva, A.K., 1973. On the motion of the geocentric radiant of the Cyclids. *Probl. Cosmic Phys. Vypusk* 8, 140–146.
- Valsecchi, G.B., Jopek, T.J., Froeschle, C., 1999. Meteoroid stream identification: A new approach – I. Theory. *Mon. Not. R. Astron. Soc.* 304, 743–750.
- Vaubailon, J. et al., 2011. The coming 2011 Draconids meteor shower. *J. Int. Meteor. Org.* 39, 59–63.
- Veres, P., Tóth, J., 2010. Analysis of the SonotaCo video meteor orbits. *J. Int. Meteor. Org.* 38, 54–57.
- Vida, D. et al., 2012. Possible new meteor shower detected from CMN and SonotaCo data. In: Gyssens, M., Roggemans, P. (Eds.), *Proceedings of the International Meteor Conference, La Palma, 20–23 September 2012*. The International Meteor Organization, Belgium, pp. 31–33.
- Whipple, F.L., 1940. Photographic meteor studies. III. The Taurid shower. *Proc. Am. Philos. Soc.* 83, 711–745.
- Whipple, F.L., 1983. 1983 TB and the Geminid meteors. In: Marsden, B.G. (Ed.), *IAU Circ. 3881*. IAU Minor Planet Center, Cambridge, MA.
- Whipple, F.L., Jacchia, L.G., 1957. Reduction methods for photographic meteor trails. *Smiths. Contrib. Astrophys.* 1, 183–206.
- Wiegert, P., Brown, P., 2005. The Quadrantid meteoroid complex. *Icarus* 179, 139–157.
- Wiegert, P. et al., 2013. The return of the Andromedids meteor shower. *Astron. J.* 145, 70–81.
- Williams, I.P., 2011. The origin and evolution of meteor showers and meteoroid streams. *Astron. Geophys.* 52, 2.20–2.26.
- Wright, F.W., Jacchia, L.G., Whipple, F.L., 1956. Photographic α -Capricornid meteors. *Astron. J.* 61, 61–69.
- Wu, Z., Williams, I.P., 1992. On the Quadrantid meteoroid stream complex. *Mon. Not. R. Astron. Soc.* 259, 617–628.
- Ye, Q. et al., 2013. Radar observations of the 2011 October Draconid outburst. *Mon. Not. R. Astron. Soc.* 436, 675–689.
- Zoladek, P., Wisniewski, M., 2012. The new July meteor shower. *J. Int. Meteor. Org.* 40, 189–194.